

October 22, 2001

## **Parameterized Direct Dynamics Study of Rate Constants of H with CH<sub>4</sub> from 250 to 2400 K**

Jingzhi Pu and Donald G. Truhlar

*Department of Chemistry and Supercomputer Institute, University of Minnesota,  
Minneapolis, MN 55455-0431*

### ***Abstract.***

Four implicit potential energy surfaces (PESs) with specific-reaction-parameters (SRP) are developed and tested for the reaction  $\text{CH}_4 + \text{H} \rightarrow \text{CH}_3 + \text{H}_2$ . The first is called MPW60 and is based on the modified Perdew-Wang (mPW) hybrid density-functional method with the percentage of Hartree-Fock (HF) exchange equal to 60%. The other three PESs are constructed with multi-coefficient correlation methods (MCCMs). The second is called MCOMP2-SRP, and the third is called MC-QCISD-SRP. Both of them are parameterized for this specific reaction by starting with their corresponding global parameters (GP). The fourth is called MCG3-SRP and is based on the MCG3-CHO semiglobal parameterization (SGP) with further refinement for this specific reaction. All four SRP surfaces have a classical forward barrier height of 14.8 kcal/mol, and all three MCCM SRP surfaces have a classical endoergicity of 3.3 kcal/mol. The stationary point geometries, vibrational frequencies, and zero-point-energies (ZPEs) are reported for several standard single-level methods and MCCMs with global parameters as well as for the four new SRP surfaces. Direct dynamics calculations are carried out using variational transition state theory (VTST) with multidimensional tunneling contributions on the proposed SRP surfaces. We calculate forward reaction rate constants for the title reaction from 250 to 2400 K and compare them with the latest re-analyzed experimental results over the temperature range from 348 to 1950 K. The calculated rate constants using canonical variational theory with the small-curvature tunneling approximation (CVT/SCT) carried out on the MPW60, MC-QCISD-SRP, and MCG3-SRP surfaces show good agreement with the experimental results.

## I. INTRODUCTION

The reaction



is an important reaction in combustion<sup>1</sup> and also serves as a prototype for radical reactions with hydrocarbons. This reaction is a subject of intense current interest for two reasons. First, Bowman *et al.*<sup>2</sup> have recently presented an apparently accurate dynamical calculation of the rate constants for a potential energy surface (PES) proposed by Jordan and Gilbert,<sup>3</sup> and we<sup>4</sup> have shown that this quantum mechanical dynamical calculation can be well reproduced by canonical variational theory<sup>5,6</sup> with the small-curvature tunneling approximation<sup>7</sup> (CVT/SCT) and the harmonic approximation in curvilinear coordinates<sup>8,9</sup> for vibrations on the same PES. If an accurate PES were available, the methods used in these calculations could apparently be used to predict accurate rate constants. Second, Sutherland *et al.*<sup>10</sup> have recently re-analyzed the experimental data for reaction (1) and its reverse in light of new thermodynamic data<sup>11</sup> for the heat of formation of methyl radical, and they were able to accommodate the best previous kinetic data<sup>12–17</sup> and their own new data<sup>10</sup> on the forward and reverse reactions by a single empirical rate expression for the rate constant  $k$  over the temperature range 348–1950 K:

$$k = B(T/T_0)^n e^{-E'/RT} \quad (2)$$

where  $B = 4.46 \times 10^{-13} \text{ cm}^3 \text{ molecule}^{-1} \text{ s}^{-1}$ ,  $T_0 = 300 \text{ K}$ ,  $n = 3.156$ , and  $E' = 8.756 \text{ kcal/mol}$ . This analysis resolves the previous inconsistencies that impeded the testing of new PESs.

The construction of analytic PESs is time-consuming and difficult, so we prefer when possible, to use direct dynamics with parameterized electronic structure methods. In direct dynamics, the PES is implicitly defined by an electronic structure level (including basis set specification) that is used to provide energies, gradients, and Hessians to the dynamics calculations on the fly.<sup>18</sup> In the present paper we report a study of reaction (1) in which we test four new specific-reaction-parameter (SRP) approaches to create an implicit PES for reaction (1).

The four SRP approaches we test are called MPWX, MCOMP2-SRP, MC-QCISD-SRP, and MCG3-SRP. We notice here that MPWX is based on the mPW hybrid density functional<sup>19</sup> that has been shown to be especially powerful for kinetics.<sup>20,21</sup> The other three SRP methods are all based on multi-coefficient correlation methods (MCCMs).<sup>22-26</sup> As part of the present study we will propose 14.8 kcal/mol as an empirical value for the classical barrier of reaction (1). All four SRP surfaces that we test below will have this empirical barrier height. Thus, by comparing these four surfaces we will be testing the effect of their difference in shape without varying the critical barrier height.

Section II presents the implicit PESs. Section III summarizes the dynamics method. Section IV presents the calculated rate constants and compares them to experiment. Section V contains concluding remarks.

## II. POTENTIAL ENERGY SURFACE

### II.A. Background on methods

Recently, a hybrid density functional method MPW1K has been parameterized to provide potential energy data for kinetics calculations.<sup>20,21</sup> In this method, the percentage of Hartree-Fock (HF) exchange is optimized to 42.8%. Its high performance-to-price ratio is impressive and makes it very promising for VTST calculations or quantum dynamics calculations.<sup>2,27-30</sup> A general scheme to improve the accuracy of the MPW1K surface for a specific reaction is to vary the percentage of HF exchange until dynamics calculations carried on the new surface yield better agreement with the experimental rate constants. In the present paper, we will present dynamics calculations based on a parameterized MPWX surface, which agrees well with a more reliable experimental measurement<sup>10</sup> for reaction (1). Another hybrid density function method called BH&HLYP has been used in previous work<sup>31</sup> for rate calculations for reaction (1). BH&HLYP is similar to MPW1K but uses different gradient-correction functionals and sets the percentage of HF exchange to 50%. The authors actually scaled the potential energy by a factor of 1.175 in their calculations employing BH&HLYP.<sup>31</sup> However,

because of the inaccuracy of the old experiments, the validity of BH&HLYP surface needs to be re-assessed, and the present paper will do so.

A series of multi-coefficient correlation methods (MCCMs) has been developed to extrapolate electronic structure calculations to include the effects of full configuration interactions and an infinite basis set. Three MCCMs studied here are (i) MCCM-CO-MP2;MG3;6-31+G(d),<sup>22,23</sup> (ii) MC-QCISD<sup>22</sup>, and (iii) MCG3<sup>24-26</sup>; these are among the highly recommended methods<sup>22</sup> and have been shown to be able to provide reasonably accurate potential energy information with affordable cost for medium- and large-sized systems. In the present paper, we label the MCCM-CO-MP2;MG3;6-31+G(d) method<sup>22</sup> as MCOMP2 for the convenience of discussion. The MCOMP2 and MC-QCISD methods are constructed from a linear combination of four components obtained from single "theory level/basis set" calculations, and the highest levels in MCOMP2 and MC-QCISD are MP2 and QCISD respectively. MCG3 is a higher-level method, which contains a linear combination of eight components and is recommended as the best MCCM method available because of its high accuracy in predicting the binding energies and geometries for various molecules.<sup>24-26</sup> In the SRP approaches proposed in this paper, the coefficients of the linear combinations for above MCCMs can be varied to obtain a more realistic barrier height or dynamics results that agree better with experiments. We note that an advantage of MCCM methods is that one can optimize geometries (including transition states) at the multi-level level,<sup>26</sup> and in this paper we use this feature, thereby avoiding the disadvantages of using single-point energies at lower-level geometries.

In next section, we will present procedures for varying the parameters in the MPW1K, MCOMP2, MC-QCISD, and MCG3 methods to obtain surfaces with a classical barrier of 14.8 kcal/mol, which was arrived at by comparing the rate constant predictions of a series of calculations with preliminary SRP surfaces to the experimental rate constants. We will not present full details of these preliminary calculations, but instead we present full sets of results with the four final SRP surfaces.

## II.B. Parameterization of the SRP surfaces

In the standard methods mentioned above, the percentage of HF exchange or the values of the multilevel coefficients are optimized against a training set. These parameters are labeled as global parameters (GP). One attempts to ensure the physical soundness of the global parameters by careful selection of the training set and by the accuracy of the thermodynamics data present in the database. When we study a specific chemical reaction, an improvement can be made by fitting a set of specific reaction parameters (SRP) against experimental data available for that specific reaction. The advantage of the SRP approach is that a set of carefully constructed specific reaction parameters close to the global parameters will, at the same time, both inherit the physical significance of the global parameters and give a better prediction for the specific reaction.

First we consider varying the parameters in the MPW1K method. In this method, the one parameter adjusted for kinetics is the percentage of HF exchange, which is set to 42.8% in the general parameterization.<sup>20,21</sup> If we vary this percentage, we obtain a series of implicit PESs denoted by MPW $X$ , where the percentage of HF exchange is  $X$ . Thus MPW42.8 is identical to MPW1K. The MPW42.8 method gives a forward barrier height of 13.6 kcal/mol. This barrier height on the MPW42.8 surface is much lower than that of the most complete available *ab initio* calculation at the CCSD(T)/cc-pVQZ//CCSD(T)/cc-VQZ level, which yields a barrier height of 15.3 kcal/mol.<sup>32</sup> Dynamics calculations carried out as part of the present study show that the rate constants calculated employing MPW42.8 are much higher than the experimental values over the temperature range of 348–1950 K,<sup>33</sup> indicating that the barrier height is underestimated on the MPW42.8 surface. To increase the classical barrier height and hence obtain better agreement with experiment, we increase the percentage of HF exchange to 60% in the SRP parameterization. The MPW60 surface yields a classical barrier height of 14.8 kcal/mol. Further parameterization of MPW $X$  can be carried out by changing this HF exchange percentage along a fine grid to get improved dynamics results. By trial and error, we find that MPW58 give the best prediction of the experimental rate constants,

and the MPW58 surface has a classical barrier height of 14.6 kcal/mol.<sup>33</sup> However, our goal here is not to optimize every method fully but rather to compare four surfaces with the same barrier height. Furthermore, the consideration of a broader set of methods led us to conclude that 14.8 kcal/mol is our best estimate of the barrier height (i.e., MPW58 may lead to better agreement with experiment by cancellation of errors rather than because it necessarily has a more accurate barrier height). Thus, we will limit our discussion in the text to the MPW60 surface. The dynamics results for MPW58 can be found in the supporting information<sup>33</sup> for readers with specialized interests.

The parameterizations of three MCCMs surface are more complicated. In each case we adjust two parameters not only to obtain a barrier of 14.8 kcal/mol but also to have a classical endoergicity  $\Delta E$  of 3.3 kcal/mol. This proposed endoergicity is obtained from eqs. (2) to (4) as follows:

$$\Delta_r H_0^0 = D_0(\text{CH}_3\text{-H}) - D_0(\text{H}_2) \quad (2)$$

$$\Delta\text{ZPE} = \text{ZPE}(\text{CH}_3) + \text{ZPE}(\text{H}_2) - \text{ZPE}(\text{CH}_4) \quad (3)$$

$$\Delta E = \Delta_r H_0^0 - \Delta\text{ZPE} \quad (4)$$

where  $\Delta_r H_0^0$  denotes a standard enthalpy change of reaction at 0 K,  $D_0$  and ZPE denote the 0 K dissociation energy and the zero-point-energy respectively, and  $\Delta E$  denotes the Born-Oppenheimer energy of reaction. The experimental data<sup>11,34,35</sup> for quantities involved in eqs. (2) to (4) are listed in Table 1. The dissociation energy of CH<sub>3</sub>-H is obtained from a recent measurement where the heat of formation of the methyl group is re-evaluated.<sup>11</sup>

Because the experimental ZPE for the CH<sub>3</sub> molecule is not available, we estimate it semiempirically from the experimental ZPE of CH<sub>4</sub> and scaled MP2/cc-pVDZ harmonic vibrational frequencies. Since the ZPE of a molecule is not a direct observable, it is obtained by using an anharmonic spectroscopic fit<sup>36</sup> to the experimental energy level spacings; such a fit then yields the ZPE. The scaling factor  $\alpha$  for the MP2/cc-pVDZ calculations is calculated as the ratio of the experimental ZPE<sup>34</sup> of CH<sub>4</sub> to the ZPE of

CH<sub>4</sub> calculated at the MP2/cc-pVDZ level using eq. (5), and ZPE of CH<sub>3</sub> is computed using eq. (6):

$$\alpha = \frac{\text{ZPE}(\text{CH}_4)_{\text{exp. (Ref.33)}}}{\text{ZPE}(\text{CH}_4)_{\text{MP2/cc-pVDZ}}} \quad (5)$$

$$\text{ZPE}(\text{CH}_3) = \alpha[\text{ZPE}(\text{CH}_3)_{\text{MP2/cc-pVDZ}}] \quad (6)$$

The resulting value of the scale factor is 0.9726, which is similar to an average value of 0.9790 determined previously<sup>37</sup> from a training set of 13 molecules.

Because of the similarity in the parameterization of MCOMP2, MC-QCISD, and MCG3, here we only present the details of obtaining the MC-QCISD-SRP parameterization as an example. For the purpose of brevity, in the following discussions, we will use the pipe "|" notation developed in our previous studies<sup>22,23</sup>, which is defined by eqs. (7)-(9):

$$\Delta E(\text{L2} | \text{L1/B}) \equiv E(\text{L2/B}) - E(\text{L1/B}) \quad (7)$$

$$\Delta E(\text{L/B2} | \text{B1}) \equiv E(\text{L/B2}) - E(\text{L/B1}) \quad (8)$$

$$\Delta E(\text{L2} | \text{L1/B2} | \text{B1}) \equiv E(\text{L2/B2}) - E(\text{L1/B2}) - [E(\text{L2/B1}) - E(\text{L1/B1})] \quad (9)$$

where L1 and L2 denote levels of theory, B1 and B2 denote basis sets. Then the MC-QCISD energy can be expressed as:<sup>22</sup>

$$\begin{aligned} E(\text{MC-QCISD}) &= c_0 E(\text{HF/6-31G(d)}) + c_1 \Delta E(\text{MP2} | \text{HF/6-31G(d)}) \\ &\quad + c_2 \Delta E(\text{MP2/MG3} | \text{6-31G(d)}) \\ &\quad + c_3 \Delta E(\text{QCISD} | \text{MP2/6-31G(d)}) \end{aligned} \quad (10)$$

where  $c_0$ – $c_3$  are called multilevel coefficients. The SRP fitting is accomplished as follows. First, we start from the MC-QCISD minimal version global parameters (MC-QCISD-v2m-GP),<sup>22</sup> and we optimize all stationary points (reactants, products, and the saddle point) using the multilevel optimization algorithm.<sup>26</sup> We describe this preliminary procedure as MC-QCISD-v2m-GP//ML. Here the notation "//ML" is used to denote that the geometries are obtained by the corresponding multilevel method on the left side of the double slash.<sup>26</sup> The MC-QCISD-v2m-GP//ML surface has a classical forward barrier height of 15.4 kcal/mol and a reaction energy of 2.1 kcal/mol as shown in Table 4.

Because the MC-QCISD energy is a linear combination of four components, the forward barrier height at a given set of geometries can be expressed as the linear combinations of the barrier height components weighted by the four multilevel coefficients from  $c_0$  to  $c_3$ . The reaction endoergicity can also be expressed as a linear combination of the results at the individual levels. In actuality the geometries depend on level, but that detail is ignored during the parameterization. We fix the first coefficient, namely  $c_0$  in GP, which corresponds to the HF part of the energy with a small basis set, to maintain the stability of the physical sense obtained from the GP. Then, we chose two of the remaining three coefficients to vary. The values of the two selected parameters to be varied can be computed by solving a 2-dimensional linear system to get the desired forward barrier height (14.8 kcal/mol) and the reaction energy (3.3 kcal/mol). Of the various possible combinations of two parameters to vary, we select the pair that leads to the smallest root-mean-square-deviation (RMSD) of the new coefficients from their corresponding GP values, i.e., we vary the two coefficients to which the results are most sensitive. The purpose of this consideration is that we try to obtain a set of balanced parameters deviating as little as possible from the general ones. The union of the optimized values of these two most sensitive coefficients with GP values of the other coefficients is proposed as the final SRP set. For MC-QCISD, we find that the coefficients for the MP2 | HF/6-31G(d) and MP2/MG3 | 6-31G(d) components, namely  $c_1$  and  $c_2$ , are the most sensitive coefficients. In MC-QCISD-SRP, both  $c_1$  and  $c_2$  are increased a little compared with their GP counterparts. The former tends to increase the reaction energy, and the latter increases the barrier height.

In dynamics calculations carried on the MC-QCISD-SRP surface, all stationary points are re-optimized at the MC-QCISD-SRP//ML level. Our calculation shows that even though the parameterization is carried out at MC-QCISD-v2m-GP//ML geometries, use of the geometries re-optimized with SRP does not perturb the barrier height and the reaction energy by more than 0.02 kcal/mol, which is not surprising considering the small size of the deviation of SRP from GP.

The parameterizations of MCOMP2 and MCG3 follow the same procedure that we have just presented for MC-QCISD. An important difference in the parameterization of MCG3 is that we start from the MCG3 semiglobal parameters<sup>38</sup> (SGP) instead of from the global parameters (v2m-GP).<sup>22</sup> Because this semiglobal parameterized version of MCG3 method was optimized for  $C_xH_yO_z$  training set molecules, we label it as MCG3-CHO-SGP. (The SGP was previously called SRP, where SRP denoted specific-range parameters. In the present paper, to avoid confusion, we use SRP only to denote specific-reaction parameters, and specific-range parameters are labeled as SGP.) All coefficients for MCOMP2, MC-QCISD, and MCG3, both in the SRP and GP versions (CHO semiglobal version for MCG3), are listed in Table 2.

### III. DETAILS OF DYNAMICS CALCULATIONS

The scaling mass for all coordinates is set equal to 1 amu. The minimum energy path (MEP) in isoinertial coordinates is followed by the Euler steepest-descent method combined with reorientation of the dividing surface (ESD/RODS) algorithm<sup>39,40</sup> in a gradient step size of  $0.01 a_0$  and with the Hessian being calculated every 9 steps. In the present study, a converged reaction path is calculated from  $-1.5 a_0$  on the reactant side to  $+1.5 a_0$  on the product side. The generalized normal mode analysis of vibrations at Hessian points along the reaction path is implemented using a set of redundant curvilinear internal coordinates.<sup>8,9</sup> The vibrational frequencies for reactants and products are also calculated in internal coordinates, which are obtained by splitting the whole set of redundant curvilinear internal coordinates into corresponding sub-sets applicable to each species. The reaction rate constants are calculated using canonical variational theory (CVT)<sup>5,6</sup> with multidimensional tunneling in the small-curvature tunneling (SCT)<sup>7</sup> approximation. The details of CVT/SCT calculations can be found elsewhere.<sup>5-7,41</sup> All dynamics calculations on multilevel implicit potential energy surfaces are done using the computer program MULTILEVELRATE,<sup>42</sup> which interfaces the VTST/multidimensional-tunneling program POLYRATE<sup>43</sup> to the electronic structure program MULTILEVEL.<sup>44</sup> The

calculations on MPWX surfaces are carried out using GAUSSRATE.<sup>45</sup> All single-level electronic structure calculations are carried out with GAUSSIAN98.<sup>46</sup>

## IV. RESULTS AND DISCUSSION

### IV. A. Stationary point properties

Before considering the full potential energy surface we first consider several calculations of the stationary points, i.e., the reactants, saddle point, and products. We will present results obtained by several standard methods (MPW1K,<sup>20</sup> MCOMP2,<sup>22,23</sup> MC-QCISD,<sup>22</sup> MCG3<sup>24-26</sup>, and MCG2<sup>24,25</sup>) as well as the SRP surfaces based on changing parameters in the MPW1K, MCOMP2, MC-QCISD, and MCG3 methods. Note that in this paper the standard MCCMs labeled without any suffix implicitly denote the corresponding methods using the version-2 minimal global parameters (v2m-GP) developed previously.<sup>22</sup> The transition state geometries and vibrational frequencies are shown in Table 3. The barrier heights, and reaction energies and the ZPE of stationary points are given in Table 4. The vibrational frequencies for reactants and products are listed in Table 5.

For systems that do not contain any atoms heavier than F, our most accurate MCCM method is MCG2.<sup>24,25</sup> Even though its high cost makes it impractical to perform dynamics calculations on this surface, we will still present the stationary points on the MCG2 surface as a benchmark to examine the accuracy of other MCCMs investigated in the present paper. Several other investigations on reaction (1) applying *ab initio* electronic structure methods have been reported in literature.<sup>31,32,47,48</sup> From those works, we select three for comparison: (1) a hybrid HF density functional method with 50% HF exchange, namely BH&HLYP,<sup>31</sup> in which a different gradient-corrected exchange functional and correlation functional from the MPWX method is used, and other two high level post-HF methods, (2) QCISD/6-311G(d,p)<sup>47</sup> and (3) CCSD(T)/cc-VQZ.<sup>32</sup> The latter method is the highest single-level calculation reported previously for

the CH<sub>4</sub> + H system. We also list the results of these calculations in Tables 3-5 for comparison.

Note that results of a more complete "double slash" calculation are available at the CCSD(T)/cc-pVQZ//CCSD(T)/cc-VQZ level.<sup>32</sup> However, in the investigation of stationary points, we select the corresponding "single slash" method at the CCSD(T)/cc-VQZ level as the highest level for comparison because all stationary point geometries and vibrational frequencies are obtained from that latter level.

#### IV.A.1. Transition state geometries and imaginary frequencies

The key geometric parameters we investigate are the length of the breaking-bond (C-H) and that of the making-bond (H-H) in the transition state of CH<sub>4</sub> + H. These are sensitive indicators of the location of the saddle point and hence are correlated with the barrier height to some extent. We also include the sum of the bond lengths of the breaking- and making-bonds in our discussion; this quantity is called perpendicular looseness, and it measures the looseness of the transition state structure in a direction perpendicular to the reaction coordinate.<sup>21</sup> In our previous work, a multilevel optimization algorithm applied to multilevel methods such as MCG3 and MC-QCISD has proved to be able to provide accurate prediction of geometries for stable molecules<sup>26</sup> and for transition states.<sup>49</sup>

In the present work, for the saddle point, MCG3 gives an H-H making-bond distance of 0.905 Å and a C-H breaking-bond distance of 1.387 Å. Compared with CCSD(T)/cc-VQZ, which gives a C-H bond length of 1.393 Å,<sup>32</sup> MCG3 provides an earlier transition state. Because of the semiempirical characteristics of the methods, the performance of MCCMs also depends on the choice of the database on which the multilevel coefficients were parameterized. Thus, we also test the semiglobal parameterized (SGP) version of MCG3 method with specific-range-parameters for C<sub>x</sub>H<sub>y</sub>O<sub>z</sub> training set molecules. We label this method as MCG3-CHO-SGP, because the composition of training molecules are limited to contain only C, H, and O. For such an SGP method, improved physical

significance of the multilevel coefficients is expected when the method is applied to a hydrocarbon system such as CH<sub>5</sub>. Interestingly, the MCG3-CHO-SGP and CCSD(T)/cc-VQZ transition state geometries agree very well in terms of both the making-bond distance and the breaking-bond distance.

The MC-QCISD method also predicts an earlier transition state by giving a C-H bond length of 1.385 Å. This may be due to the less complete extrapolation of the electron-correlation energy in MC-QCISD (MC-QCISD only has four components compared to eight components in MCG3). It is a good practice to compare the MC-QCISD geometry with the QCISD geometry, because the latter is the highest level of electron correlation in MC-QCISD, in which efficiency is achieved by avoiding the combination of QCISD with a large basis set. MC-QCISD and QCISD/6-311G(d,p) give the same making-bond distance of 0.899 Å and slight difference of 0.005 Å for the breaking-bond distance at the saddle point. This agreement may be treated as an evidence for the inheritance of the QCISD characteristics in the MC-QCISD method, even though the latter only contains a small-basis QCISD component.

MPW1K gives a saddle point geometry that is only slightly different from the pure *ab initio* methods. When the percentage of HF exchange is increased to 60% in the MPW60 calculation, there is a very significant decrease from 1.401 Å to 1.388 Å in the breaking-bond length. This decrease results in a tighter transition state with a perpendicular looseness of 2.277 Å on the MPW60 surface.

In the listed methods, the MCOMP2 method displays the most systematic errors in the transition state geometries by underestimating both the breaking-bond and the making-bond distances, hence giving a smaller perpendicular looseness, corresponding to a tight transition state. This underestimate possibly comes from the bad geometry predictions<sup>22</sup> of the MP2 component.

The systematic error in MCOMP2 method is also reflected in the imaginary frequencies of the saddle point. Both MCOMP2 and MCOMP2-SRP surfaces give an imaginary frequency around 1550i cm<sup>-1</sup>, while for other MCCMs examined in this paper,

this quantity ranges from  $1332i$  to  $1480i$   $\text{cm}^{-1}$ . Hybrid HF density functional methods tend to give a lower imaginary frequency than *ab initio* methods. By increasing the percentage of HF exchange, this imaginary frequency is also increased. For example, the MPW1K surface in which the HF exchange is set to 42.8% has an imaginary frequency of  $1302i$   $\text{cm}^{-1}$ , while in MPW60, with HF exchange increased to 60%, the imaginary frequency is increased to  $1458i$   $\text{cm}^{-1}$ . The imaginary frequency for BH&HLYP, in which HF exchange is weighted 50%, is  $1411i$   $\text{cm}^{-1}$ , which is between MPW1K and MPW60. Even though it uses a different gradient-corrected exchange and correlation functional than the MPWX series, the general trend is that mixing in a higher percentage of HF exchange introduces a high imaginary frequency. Too high of an imaginary frequency would indicate too large of a negative force constant for the reaction coordinate mode at the saddle point and hence too thin of a barrier, which would introduce systematic overestimates of the tunneling probability in dynamics calculations. Our best estimate of the imaginary frequency would be between  $1300i$  and  $1500i$   $\text{cm}^{-1}$ . All our proposed SRP methods except MCOMP2-SRP have imaginary frequencies falling into this range.

#### IV.A.2. Barrier heights

Table 4 shows forward barrier heights ( $V_{\ddagger}^{\ddagger}$ ) and reverse barrier heights ( $V_{\ddagger}^{\ddagger}$ ) on the proposed SRP surfaces. MPW1K and BH&HLYP give forward barrier heights of 13.3 and 12.6 kcal/mol; both are lower than our best estimate. We found that pure density functional methods (such as BLYP<sup>50</sup> and mPWPW91<sup>19</sup>) tend to underestimate the reaction barrier heights.<sup>20</sup> On the other hand, HF theory usually overestimates the barrier heights. In our hybrid HF-density-functional methods with SRP, the barrier height is adjusted so that the rate constants for reaction (1) agree with carefully re-analyzed experimental results.<sup>10</sup> It has been shown that we have to increase the percentage of HF exchange to around 58–60%. The MPW60 surface has a forward barrier height of 14.8 kcal/mol. We note that Truong and Duncan scaled the BH&HLYP barrier by 1.175 in

their dynamics calculations, actually also using a barrier height of 14.8 kcal/mol. If a similar strategy of increasing the percentage of HF exchange in BH&HLYP is used to get this barrier height, an adjusted percentage even greater than 60% (up to 80%, as determined by our own calculation) is needed, as expected because MPW1K with 42.8% HF exchange already has a higher barrier height than BH&HLYP with 50% HF exchange.

A high percentage of HF exchange has disadvantages as a trade-off for the improvement in the prediction of the reaction barrier height. First, the accuracy of prediction of binding energies might be diminished, and hence the prediction of the energy of reaction may deteriorate. To examine whether the proposed forward barrier height of the MPW60 method is accurate and to provide the most accurate possible implicit PES for this important prototype reaction, we also developed three SRP surfaces based on MCCMs with the same barrier height of 14.8 kcal/mol. For MCCM methods in which we vary more than one parameter, the parameterization strategy described above allows us to get the proposed forward barrier height and the correct reaction energy at the same time. This provides us with an opportunity to examine the effect of the different shapes of four surfaces with the same critical barrier height by comparing their dynamics predictions. The second negative effect of too much HF exchange is that the vibrational frequencies may be too high, as well as giving too high of an imaginary frequency. The first effect may prevent us from getting the correct reverse barrier heights even if we adjust the forward barrier height to a reasonable value. The high frequency effects may be masked because of cancellations of ZPE for both reactants and the transition state; we will return to this point in the next subsection.

As mentioned above, we propose our best estimate of the barrier height of reaction (1) as 14.8 kcal/mol in the present paper. This best estimate is in excellent agreement with three of our best generally parameterized MCCMs, i.e., MCG3, MCG3-CHO-SRP, and MCG2, which give forward barrier heights of 14.9, 15.1, and 14.7 kcal/mol respectively. We also note that this proposed barrier height is in reasonable agreement

with the most complete *ab initio* calculation at the CCSD(T)/cc-pVQZ//CCSD(T)/cc-VQZ level, which has a forward barrier height of 15.3 kcal/mol.<sup>32</sup>

#### IV.A.3. Vibrational frequencies for reactants and products

Vibrational frequencies for the reactants and products on the proposed PESs are listed in Table 5. MPWX hybrid HF density functional methods overestimate the frequencies compared to experimental<sup>35,36,51</sup> values. This overestimate gets worse when the percentage of HF exchange is increased. The same trend is displayed for the BH&HLYP method, and this overestimate can be ascribed to using too much HF exchange. It is known that the harmonic frequencies obtained at the HF level are overestimated by 10–20%.<sup>52</sup> This overestimate can be relieved if we scale all frequencies by a factor smaller than one, and such scaling is also expected to improve dynamics predictions. For example, we find that dynamics calculations carried out on the MPW60 surface using frequencies scaled by 0.96 reproduce experimental rate constants better than using unscaled frequencies on the same surface.<sup>33</sup>

Most multilevel methods in Table 5 give good frequencies, except that the MCOMP2 and the MCOMP2-SRP surfaces overestimate the frequencies. The major reason for this overestimate is that in MCOMP2 the extrapolation to include electron correlation is truncated at the MP2 level. Frequencies at the MP2 level are expected to be overestimated by about 5%.<sup>52</sup> Thus we propose that the presence of a QCISD component in MC-QCISD is important to improve the frequencies prediction compared with a method having only HF and MP2 components, such as MCOMP2. It is very encouraging that MC-QCISD frequencies are in good agreement with MCG3, which is the most accurate MCCM method. The semiglobal parameterized MCG3 with specific-range-parameters, namely MCG3-CHO-SGP, makes a further improvement in predicting the H<sub>2</sub> frequency. MC-QCISD, MCG3, and MCG3-CHO-SGP frequencies are in good agreement with the most accurate single-level calculation at the CCSD(T)/cc-VQZ level and with the experimental values. We find that the MC-QCISD frequencies are similar to

QCISD/6-311G(d,p) frequencies, even though the largest basis set used for QCISD component in MC-QCISD is 6-31G(d). Thus the combination of a QCISD component with lower-level calculations in MC-QCISD seems to inherit the improved QCISD frequency characteristics at the same time as it improves the barrier height prediction as compared to that from a single QCISD calculations.

#### IV.B. Potential energy and effective potential along the reaction path

Figure 1 shows the potential energy along the minimum energy path; this potential curve is called  $V_{\text{MEP}}$ . We can see that the MPW60 barrier and the MCOMP2-SRP barrier are thinner than those of the MC-QCISD-SRP and MCG3-SRP surfaces as prefigured by the higher imaginary frequencies at the saddle point for the first two SRP surfaces. Figure 2 shows the ground-state vibrationally adiabatic potential energy curve,  $V_a^{\text{G}}$ , as a function of reaction coordinate  $s$  for the proposed four SRP surfaces; this is obtained by adding the local zero point energy to  $V_{\text{MEP}}$ . The potential energies along the  $V_a^{\text{G}}$  curve for MPW60 surface are higher than those of other three MCOMs SRP surfaces. This difference can be ascribed to a systematic overestimate of vibrational frequencies on the MPW60 surface.

#### IV.C. Reaction rate constants

Reaction rate constants for 250–2400 K obtained from dynamical calculations based on four SRP surfaces and corresponding experimental values are given in Table 6. To analyze the variational and tunneling effects, we list rate constants for several dynamical levels: conventional transition-state theory (TST), canonical variational transition-state theory (CVT), and CVT with multi-dimensional tunneling contributions in the small curvature tunneling approximation (CVT/SCT). The Arrhenius plots for the calculated CVT/SCT rates on the four SRP surfaces and the experimental expression over 348–1950 K are shown in Figure 3. Because all our proposed SRP surfaces have the same forward classic barrier height (14.8 kcal/mol), the comparison of the dynamics behavior on these

surfaces provides important information about the effect of varying the shape of the surfaces. To illustrate this comparison, we further analyze the ratio of the CVT rate to the TST rate on our proposed SRP surfaces; this shows the variational effects in dynamics calculations carried on these surfaces. Additionally, we compute the ratio of the CVT/SCT rate to the CVT rate to elucidate the relative role of tunneling contributions. Those ratios of rate constants are presented in Table 7.

Table 6 shows that the MPW60 surface predicts dynamics results in good agreement with experiment over the whole temperature range. The deviation from experiment is no more than 13%, except for deviations of -26% and -22% at the two low-temperature points. Considering the possibility of inaccurate extrapolations over insufficient experimental points at low temperatures, our dynamics calculations on the MPW60 surface are judged successful. We also note that the rate constants on the MPW60 surface are actually underestimated over the temperature region in the present study, which indicates that a reduced barrier height lower than 14.8 kcal/mol may further improve the dynamics results. A better dynamics result can be obtained on the MPW58 surface with a barrier height of 14.6 kcal/mol.<sup>33</sup>

The MCOMP2-SRP surface tends to overestimate the rate constants over the whole temperature region under investigation, suggesting (if it were the best calculation we have) that the actual barrier may be a little higher than 14.8 kcal/mol. However, MCOMP2-SRP makes a better prediction than other methods at lower temperatures. We ascribe this to an overestimate of the tunneling on MCOMP2 surface because it has a thin barrier with a high imaginary frequency at the saddle point. The quantitative evidence of this overestimate of tunneling can be seen from the ratio of the CVT/SCT rate to the CVT rate on the MCOMP2-SRP surface in Table 7.

The dynamics behavior on the MC-QCISD-SRP surface shows a different trend than that on MPW60 or MCOMP2-SRP surfaces. It underestimates the rates at low temperatures but overestimates the rates at high temperatures.

The MCG3-SRP surface is the highest-level method of the four SRP surface candidates. We have observed from the above discussion that MCG3-SRP surface can provide good saddle point geometries and is able to reproduce vibrational frequencies at stationary points in agreement both with the most complete single-level calculation and with experiments. The performance of the dynamics calculations on this surface is also encouraging, especially its ability to predict the rate constants at low temperatures. The deviations from experiment at 348 and 400 K are only -13% and -11% respectively. The average deviation of the MCG3-SRP rate constants from experiment is 14% for 348–800 K, 23% for 900–1500 K, and 15% for 1600–1950 K, for an overall average of 17%.

In the low-temperature region, tunneling effects are expected to be prominent, and indeed we do find large tunneling there. In particular, Table 6 shows that both TST and CVT without tunneling contributions give poor predictions of the reaction rate at low temperatures. The ratio  $k^{\text{CVT/SCT}}/k^{\text{CVT}}$  for MCG3-SRP is 41.0, 11.3, 10.9, and 5.4 at 250, 298, 300, and 348 K, respectively.

#### IV. D. Activation energy $E_a$

The activation energies  $E_a$  are calculated from rate constants at two temperatures:

$$E_a = R \frac{T_1 T_2}{T_1 - T_2} \ln \frac{k(T_1)}{k(T_2)} \quad (9)$$

where  $R$  is the gas constant,  $T_1$  and  $T_2$  are a pair of temperatures, and  $k(T_1)$  and  $k(T_2)$  are the rate constant at each temperature. To investigate the temperature dependence of dynamics calculations carried out on various PESs, we examine such two-point activation energies over the temperature range from 250–2400 K. The results are given in Table 8. For a systematic and meaningful comparison, experiment activation energies are calculated in precisely the same way using the experimental rate constant expression (2) and are also shown in Table 8.

Over a wide temperature region, the phenomenological activation energy varies from  $\sim 9$  kcal/mol up to  $\sim 20$  kcal/mol. This variation results from the concave shape of

the Arrhenius curves. There is a dangerous assumption in many papers that the experimental activation energy provides a good indicator of the classical reaction barrier height. In light of the large temperature dependence of the activation energy, one sees that it is inappropriate to adjust the classical barrier height in a dynamics calculation to agree with the activation energy reported experimentally.

The temperature dependence of the phenomenological  $E_a$  is usually called "Arrhenius curvature". Table 8 shows that the experimental  $E_a$  rises by 4.5 kcal/mol from 348–800 K to 800–1950 K. In contrast our four SRP values are all in the range of 3.7–4.0 kcal/mol. Thus, theory gives less curvature than experiment, which is also evident in Figure 3. Adding recrossing in a transmission coefficient would lower the predicted rate constants more at high  $T$  than at low  $T$  and decrease the predicted curvature. Thus the main possibilities for why theory underestimates the curvature are: (i) lack of explicit anharmonicity in the theory, (ii) not enough tunneling in the theory either due to the use of the SCT approximation or due to the PES shape, (iii) inaccuracies in the experiment or the fit to experiment. This is clearly a very important issue to understand (since extrapolation of limited data to a wider temperature range is a key role that theory can play), and further work to understand it would be very desirable.

## V. CONCLUDING REMARKS

In this work, we have developed four implicit potential energy surfaces with specific reaction parameters (SRP) for the reaction  $\text{CH}_4 + \text{H} \rightarrow \text{CH}_3 + \text{H}_2$  based on hybrid HF density functional theory and multi-coefficient correlation methods. All four SRP surfaces have the same classical barrier height of 14.8 kcal/mol, which is our best estimate for this reaction. The parameterizations of three of the surfaces are also designed to reproduce the experimental reaction energy, which has been estimated from experiment to be 3.3 kcal/mol by using re-assessed thermodynamics data<sup>11</sup> for the methyl group.

First we investigated stationary point properties on our SRP surfaces and compared them with high-level calculations reported previously. We noted a systematic overestimate of frequencies for the hybrid HF density functional theory method when the fraction of HF exchange is high. Three of our SRP surfaces give good predictions of saddle point geometry, but the MCOMP2-SRP surface gives too tight of a transition state. It is very encouraging that three of our highest-level MCCM methods predict a classical barrier in the range 14.7–15.1 kcal/mol, in very good agreement with our best estimate.

Secondly, we carried out direct dynamics calculations on the four proposed surfaces using canonical variational transition state theory with the small-curvature tunneling approximation (CVT/SCT). The calculated reaction rate constants are compared with the re-analyzed experimental results for the title reaction from 348 K to 1950 K. The dynamics results for the MPW60, MC-QCISD-SRP, and MCG3-SRP implicit potential energy surfaces are all in good agreement with experiment. Thus, these methods are all good candidates for future direct dynamics calculations that might be used to predict state-to-state cross sections, kinetic isotope effects, or other more detailed dynamical quantities.

## **ACKNOWLEDGMENTS**

This work was supported in part by the U.S. Department of Energy, Office of Basic Energy Sciences.

**Reference**

- <sup>1</sup>J. Warnatz, in *Combustion Chemistry*, edited by W. C. Gardiner, Jr. (Springer-Verlag, New York, 1984), p. 233.
- <sup>2</sup>J. M. Bowman, D. Wang, X. Huang, F. Huarte-Larrañaga, and U. Manthe, *J. Chem. Phys.* **114**, 9683 (2001).
- <sup>3</sup>M. J. T. Jordan, and R. G. Gilbert, *J. Chem. Phys.* **102**, 5669 (1995).
- <sup>4</sup>J. Pu, J. C. Corchado, and D. G. Truhlar, *J. Chem. Phys.*, submitted.
- <sup>5</sup>B. C. Garrett and D. G. Truhlar, *J. Chem. Phys.* **70**, 1593 (1979).
- <sup>6</sup>D. G. Truhlar, A. D. Isaacson, R. T. Skodje, and B. C. Garrett, *J. Phys. Chem.* **86**, 2252 (1982).
- <sup>7</sup>Y.-P. Liu, G. C. Lynch, T. N. Truong, D.-H. Lu, D. G. Truhlar, and B. C. Garrett, *J. Am. Chem. Soc.* **115**, 2408 (1993).
- <sup>8</sup>C. F. Jackels, Z. Gu, and D. G. Truhlar, *J. Chem. Phys.* **102**, 3188 (1995).
- <sup>9</sup>Y.-Y. Chuang and D. G. Truhlar, *J. Phys. Chem. A* **102**, 232 (1998).
- <sup>10</sup>J. W. Sutherland, S.-C. Su, and J. V. Michael, *Int. J. Chem. Kinet.*, in press.
- <sup>11</sup>B. Ruscic, M. Litorja, and R. L. Asher, *J. Phys. Chem. A* **103**, 8625 (1999).
- <sup>12</sup>K. Wintergerst, and P. Frank, Abstracts, 12th Int. Symp. on Gas Kinetics, paper E40, Reading, England, July, 1992.
- <sup>13</sup>M. J. Rabinowitz, J. W. Sutherland, P. M. Patterson, and R. B. Klemm, *J. Phys. Chem.* **95**, 674 (1991).
- <sup>14</sup>P.-M. Marquaire, A. G. Dastidar, K. C. Manthorne, and P. D Pacey, *Can. J. Chem.*, **72**, 600 (1994).
- <sup>15</sup>H. J. Baeck, K. S. Shin, H. Yang, Z. Qin, V. Lissianski, and W. C. Gardiner, Jr., *J. Phys. Chem.* **99**, 15925 (1995).
- <sup>16</sup>V. D. Knyazev, A. Bencsura, S. I. Stoliarov, and I. R. Slagle, *J. Phys. Chem.* **100**, 11346 (1996).
- <sup>17</sup>M. G. Bryukov, I. R. Slagle, and V. D. Knyazev, *J. Phys. Chem. A* **105**, 3107 (2001).

- <sup>18</sup>D. G. Truhlar, in *The Reaction Path in Chemistry: Current Approaches and Perspectives*, edited by D. Heidrich (Kluwer, Dordrecht, 1995), p. 229.
- <sup>19</sup>C. Adamo and V. Barone, *J. Chem. Phys.* **108**, 664 (1998).
- <sup>20</sup>B. J. Lynch, P. L. Fast, M. Harris, and D. G. Truhlar, *J. Phys. Chem. A* **104**, 4811 (2000)
- <sup>21</sup>B. J. Lynch and D. G. Truhlar, *J. Phys. Chem. A* **105**, 2936 (2001).
- <sup>22</sup>P. L. Fast and D. G. Truhlar, *J. Phys. Chem. A* **104**, 6111 (2000).
- <sup>23</sup>P. L. Fast, J. C. Corchado, M. L. Sánchez, and D. G. Truhlar, *J. Phys. Chem. A* **103**, 5129 (1999).
- <sup>24</sup>C. M. Tratz, P. L. Fast, and D. G. Truhlar, *Phys. Chem. Comm.* **2/14**,1 (1999).
- <sup>25</sup>P. L. Fast, M. L. Sánchez, and D. G. Truhlar, *Chem. Phys. Lett.* **306**, 407 (1999).
- <sup>26</sup>J. M. Rodgers, P. L. Fast, and D. G. Truhlar, *J. Chem. Phys.* **112**, 3141 (2000).
- <sup>27</sup>T. Takayanagi, *J. Chem. Phys.* **104**, 2237 (1996).
- <sup>28</sup>H.-G. Yu and G. Nyman, *J. Chem. Phys.* **111**, 3508 (1999).
- <sup>29</sup>H.-G. Yu, *Chem. Phys. Lett.* **332**, 538 (2001).
- <sup>30</sup>F. Huarte-Larrañaga, and U. Manthe, *J. Chem. Phys.* **113**, 5115 (2000).
- <sup>31</sup>T. N. Truong and Wendell Duncan, *J. Chem. Phys.* **101**, 7408 (1994).
- <sup>32</sup>E. Kraka, J. Gauss, and D. Cremer, *J. Chem. Phys.* **99**, 5306 (1993).
- <sup>33</sup>See EPAPS Document No. E-JCPSAx-xxx-xxxxxx. This document may be retrieved via the EPAPS homepage (<http://www.aip.org/pubservs/epaps.html>) or from <ftp.aip.org> in the directory/epaps/. See the EPAPS home page for more information.
- <sup>34</sup>J. M. L. Martin, *J. Chem. Phys.* **97**, 5012 (1992).
- <sup>35</sup>*JANAF* Thermochemical Tables (U. S. GPO, Washington, DC, 1971), Vol. 37.
- <sup>36</sup>D. L. Gray and A. G. Robiette, *Mol. Phys.* **37**, 1901 (1979).
- <sup>37</sup>P. L. Fast, J. Corchado, M. L. Sanchez, and D. G. Truhlar, *J. Phys. Chem. A* **103**, 3139 (1999).
- <sup>38</sup>P. L. Fast, N. E. Schultz, and D. G. Truhlar, *J. Phys. Chem. A* **105**, 4143(2001).

- <sup>39</sup>A. González-Lafont, J. Villà, J. M. Lluch, J. Bertrán, R. Steckler, and D. G. Truhlar, J. Phys. Chem. A **102**, 3420 (1998).
- <sup>40</sup>P. L. Fast, J. C. Corchado, and D. G. Truhlar, J. Chem. Phys. **109**, 6237 (1998).
- <sup>41</sup>D. G. Truhlar, A. D. Isaacson, and B. C. Garret, in *Theory of Chemical Reaction Dynamics*, M. Baer, Ed., CRC Press: Boca Raton, FL, 1985, Vol 4, p65.
- <sup>42</sup>J. Pu, J. C. Corchado, B. J. Lynch, P. L. Fast, and D. G. Truhlar, MULTILEVELRATE—version 8.7, University of Minnesota, Minneapolis, 2001.
- <sup>43</sup>Y. -Y. Chuang, J. Corchado, P. L. Fast, J. Villa, W. -P. Hu, Y. -P. Liu, G. C. Lynch, K. Nguyen, C. F. Jackels, M. Z. Gu, I. Rossi, E. L. Coitino, S. Clayton, V. Melissas, B.J. Lynch, E. L. Coitino, A. Frenadez-Ramos, J. Pu, R. Steckler, B. C. Garret, A. D. Isaacson, and D. G. Truhlar, POLYRATE—version 8.7, University of Minnesota, Minneapolis, 2001.
- <sup>44</sup>J. M. Rodgers, B. J. Lynch, P. L. Fast., Y -Y. Chuang, J. Pu, and D. G. Truhlar, MULTILEVEL—version 2.3, University of Minnesota, Minneapolis, 2001.
- <sup>45</sup>J. C. Corchado, Y. -Y, Chuang, E. L. Coitino and D. G. Truhlar, GAUSSRATE-version 8.7, University of Minnesota, Minneapolis, 2001.
- <sup>46</sup>GAUSSIAN98, by M. J. Frisch, G. W. Trucks, H. B. Schlegel, G. E. Scuseria, M. A. Robb, J. R. Cheeseman, V. G. Zakrzewski, J. A. Montgomery, R. E. Stratmann, J. C. Burant, S. Dapprich, J. M. Millam, A. D. Daniels, K. N. Kudin, M. C. Strain, O. Farkas, J. Tomasi, V. Barone, M. Cossi, R. Cammi, B. Mennucci, C. Pomelli, C. Adamo, S. Clifford, J. Ochterski, G. A. Petersson, P. Y. Ayala, Q. Cui, K. Morokuma, D. K. Malick, A. D. Rabuck, K. Raghavachari, J. B. Foresman, J. Cioslowski, J. V. Ortiz, B. Stefanov, G. Liu, A. Liashenko, P. Piskorz, I. Komaromi, R. Gomperts, R. L. Martin, D. J. Fox, T. Keith, M. A. Al-Laham, C. Y. Peng, A. Nanayakkara, C. Gonzalez, M. Challacombe, P. M. W. Gill, B. G. Johnson, W. Chen, M. W. Wong, J. L. Andres, M. Head-Gordon, E.S. Replogle and J. A. Pople, Gaussian, Inc., Pittsburgh PA, 1998.
- <sup>47</sup>T. N. Truong, J. Chem. Phys. **100**, 8014 (1994).

- <sup>48</sup>Y. Kurosaki and T. Takayanagi, *J. Chem. Phys.* **110**, 10830 (1999).
- <sup>49</sup>B. J. Lynch and D. G. Truhlar, unpublished work.
- <sup>50</sup>P. M. W. Gill, B. G. Johnson, J. A. Pople, and M. J. Frisch, *Int. J. Quantum Chem. Symp.* **26**, 319 (1992).
- <sup>51</sup>*NIST Chemistry WebBook*, <http://webbook.nist.gov/chemistry>.
- <sup>52</sup>W. J. Hehre, L. Random, P. v.R. Schleyer, and J. A. Pople, *Ab Initio Molecular Orbital Theory*; Wiley, New York, 1986.

Table 1. The proposed reaction endoergicity (in kcal/mol) for  $\text{CH}_4 + \text{H} \rightarrow \text{CH}_3 + \text{H}_2$ 

| Thermal Quantity            | Value  | Ref. or method   |
|-----------------------------|--------|--|
| $D_0(\text{CH}_3\text{-H})$ | 103.42 | Ref. 11  |
| $D_0(\text{H-H})$           | 103.27 | Ref. 35  |
| $\Delta_r H_0^0$            | 0.15   | $D_0(\text{CH}_3\text{-H}) - D_0(\text{H-H})$                                |
| ZPE( $\text{CH}_4$ )        | 27.71  | Ref. 34  |
| ZPE( $\text{CH}_3$ )        | 18.33  | scaled MP2/cc-pVDZ <sup>a</sup>  |
| ZPE( $\text{H}_2$ )         | 6.21   | Ref. 34  |
| $\Delta\text{ZPE}$          | -3.17  | $\text{ZPE}(\text{CH}_3) + \text{ZPE}(\text{H}_2) - \text{ZPE}(\text{CH}_4)$ |
| $\Delta E$                  | 3.32   | $\Delta_r H_0^0 - \Delta\text{ZPE}$  |

<sup>a</sup>The scaling factor is obtained by eq. (5)

Table 2. The global parameters (GP) and specific reaction parameters (SRP) for MCOMP2, MC-QCISD, MCG3, and MCG2.

|                 | $c_0$  | $c_1$  | $c_2$  | $c_3$  | $c_4$  | $c_5$  | $c_6$  | $c_7$  | $c_8$  | Ref.              |
|-----------------|--------|--------|--------|--------|--------|--------|--------|--------|--------|-------------------|
| MCOMP2-v2m-GP   | 0.9724 | 1.2936 | 0.8577 | 2.0067 |        |        |        |        |        | 22                |
| MCOMP2-SRP      | 0.9724 | 1.6893 | 0.7832 | 2.0067 |        |        |        |        |        | p.w. <sup>a</sup> |
| MC-QCISD-v2m-GP | 1.0038 | 1.0949 | 1.2047 | 1.0441 |        |        |        |        |        | 22                |
| MC-QCISD-SRP    | 1.0038 | 1.3896 | 1.3508 | 1.0441 |        |        |        |        |        | p.w.              |
| MCG3-v2m-GP     | 1.0121 | 1.2047 | 1.0646 | 1.0975 | 1.1859 | 0.8139 | 1.4470 | 1.4142 |        | 25                |
| MCG3-CHO-SGP    | 1.0054 | 0.9060 | 1.0527 | 1.2504 | 0.9272 | 0.4746 | 1.0165 | 1.5713 |        | 38                |
| MCG3-SRP        | 1.0054 | 0.9060 | 1.1038 | 1.3475 | 0.9272 | 0.4746 | 1.0165 | 1.5713 |        | p.w.              |
| MCG2-v2m-GP     | 0.9926 | 0.6149 | 1.1703 | 0.9968 | 1.0330 | 4.6485 | 0.5703 | 4.3440 | 1.2560 | 25                |

<sup>a</sup>denotes present work.

Table 3. Geometries ( $\text{\AA}$ , deg) and harmonic vibrational frequencies of the saddle point ( $\text{cm}^{-1}$ ).

| Methods             | Bond lengths |       |                  | Bond angle           | Frequencies |         |         |             |             |         |               |                | Ref.              |
|---------------------|--------------|-------|------------------|----------------------|-------------|---------|---------|-------------|-------------|---------|---------------|----------------|-------------------|
|                     | H-H          | C-H   | Sum <sup>a</sup> | $\angle\text{H-C-H}$ | $\nu_{1,2}$ | $\nu_3$ | $\nu_4$ | $\nu_{5,6}$ | $\nu_{7,8}$ | $\nu_9$ | $\nu_{10,11}$ | $\nu^\ddagger$ |                   |
| MPW1K               | 0.885        | 1.401 | 2.287            | 103.0                | 3330        | 3169    | 1927    | 1467        | 1176        | 1095    | 565           | 1302 <i>i</i>  | p.w. <sup>b</sup> |
| MCOMP2              | 0.874        | 1.380 | 2.254            | 102.9                | 3271        | 3113    | 1910    | 1430        | 1115        | 1056    | 531           | 1547 <i>i</i>  | p.w.              |
| MC-QCISD            | 0.899        | 1.385 | 2.284            | 103.2                | 3222        | 3073    | 1780    | 1420        | 1106        | 1069    | 517           | 1480 <i>i</i>  | p.w.              |
| MCG3                | 0.905        | 1.387 | 2.292            | 103.3                | 3217        | 3071    | 1739    | 1432        | 1108        | 1080    | 515           | 1397 <i>i</i>  | p.w.              |
| MCG3-CHO-SGP        | 0.901        | 1.394 | 2.295            | 103.1                | 3236        | 3087    | 1745    | 1433        | 1124        | 1073    | 530           | 1406 <i>i</i>  | p.w.              |
| MCG2                | 0.888        | 1.409 | 2.297            | 103.0                | 3196        | 3046    | 1851    | 1425        | 1121        | 1062    | 520           | 1352 <i>i</i>  | p.w.              |
| MPW60               | 0.889        | 1.388 | 2.277            | 103.1                | 3378        | 3215    | 1875    | 1496        | 1202        | 1129    | 575           | 1458 <i>i</i>  | p.w.              |
| MCOMP2-SRP          | 0.880        | 1.368 | 2.248            | 103.0                | 3258        | 3102    | 1867    | 1429        | 1089        | 1061    | 508           | 1559 <i>i</i>  | p.w.              |
| MC-QCISD-SRP        | 0.882        | 1.409 | 2.291            | 103.1                | 3202        | 3044    | 1978    | 1388        | 1052        | 1021    | 501           | 1332 <i>i</i>  | p.w.              |
| MCG3-SRP            | 0.896        | 1.398 | 2.294            | 103.0                | 3235        | 3084    | 1781    | 1427        | 1118        | 1063    | 529           | 1372 <i>i</i>  | p.w.              |
| BH&HLYP/6-311G(d,p) | 0.896        | 1.387 | 2.284            | 103.4                | 3297        | 3151    | 1807    | 1482        | 1177        | 1127    | 558           | 1411 <i>i</i>  | 31                |
| QCISD/6-311G(d,p)   | 0.899        | 1.390 | 2.289            | 103.7                | 3236        | 3090    | 1764    | 1459        | 1152        | 1111    | 534           | 1529 <i>i</i>  | 47                |
| CCSD(T)/cc-VQZ      | 0.897        | 1.393 | 2.290            | 103.7                | 3229        | 3083    | 1763    | 1458        | 1124        | 1093    | 518           | 1500 <i>i</i>  | 32                |

<sup>a</sup>Sum denotes the sum of the making bond and breaking bond distances.<sup>b</sup>p.w. denotes present work.

Table 4. ZPEs, barrier heights and reaction energies for PESs (in kcal/mol)

| Methods             | ZPE               |                   |                  |                   |                       |                       | Barrier heights             |                             |     | Ref.              |
|---------------------|-------------------|-------------------|------------------|-------------------|-----------------------|-----------------------|-----------------------------|-----------------------------|-----|-------------------|
|                     | CH <sub>4</sub>   | CH <sub>3</sub>   | H <sub>2</sub>   | S.P. <sup>a</sup> | S.P. – R <sup>b</sup> | S.P. – P <sup>c</sup> | V <sub>f</sub> <sup>‡</sup> | V <sub>r</sub> <sup>‡</sup> | ΔE  |                   |
| MPW1K               | 28.8              | 19.2              | 6.5              | 27.5              | -1.28                 | 1.9                   | 13.3                        | 9.8                         | 3.6 | p.w. <sup>d</sup> |
| MCOMP2              | 28.3              | 18.7              | 6.5              | 26.8              | -1.60                 | 1.5                   | 15.5                        | 10.8                        | 4.6 | p.w.              |
| MC-QCISD            | 28.0              | 18.7              | 6.2              | 26.4              | -1.57                 | 1.5                   | 15.4                        | 13.4                        | 2.1 | p.w.              |
| MCG3                | 28.0              | 18.7              | 6.3              | 26.4              | -1.68                 | 1.4                   | 14.9                        | 13.1                        | 1.7 | p.w.              |
| MCG3-CHO-SGP        | 28.2              | 18.7              | 6.3              | 26.5              | -1.64                 | 1.5                   | 15.1                        | 12.0                        | 3.1 | p.w.              |
| MCG2                | 27.9              | 18.5              | 6.3              | 26.4              | -1.45                 | 1.6                   | 14.7                        | 11.2                        | 3.5 | p.w.              |
| MPW60               | 29.3              | 19.5              | 6.6              | 27.9              | -1.45                 | 1.9                   | 14.8                        | 11.1                        | 3.6 | p.w.              |
| MCOMP2-SRP          | 28.2              | 18.8              | 6.4              | 26.6              | -1.39                 | 1.4                   | 14.8                        | 11.5                        | 3.3 | p.w.              |
| MC-QCISD-SRP        | 27.6              | 18.6              | 6.2              | 26.2              | -1.57                 | 1.5                   | 14.8                        | 11.5                        | 3.3 | p.w.              |
| MCG3-SRP            | 28.1              | 18.7              | 6.3              | 26.5              | -1.38                 | 1.5                   | 14.8                        | 11.5                        | 3.3 | p.w.              |
| BH&HLYP/6-311G(d,p) | 28.8 <sup>e</sup> | 18.8 <sup>e</sup> | 6.5 <sup>e</sup> | 27.3 <sup>e</sup> | -1.47                 | 2.1                   | 12.6                        | 11.2                        | 1.4 | 31                |
| QCISD/6-311G(d,p)   | 28.3              | 18.7              | 6.4              | 26.8              | -1.52                 | 1.7                   | 16.3                        | 13.8                        | 2.5 | 47                |
| CCSD(T)/cc-VQZ      | 28.3              | 18.8              | 6.3              | 26.6              | -1.69                 | 1.5                   | 15.3                        | 11.8                        | 3.5 | 32                |

<sup>a</sup>S.P. denotes saddle point.<sup>b</sup>S.P. – R denotes S.P. minus reactants.<sup>c</sup>S.P. – P denotes S.P. minus products.<sup>d</sup>p.w. denotes present work.<sup>e</sup>calculated from tabulated harmonic frequencies in Ref. 31.

Table 5. Vibrational frequencies ( $\text{cm}^{-1}$ ) for reactants and products.

|                     | CH <sub>4</sub>   |                   |                   |                   | CH <sub>3</sub>   |                  |                   |                   | H <sub>2</sub>    |
|---------------------|-------------------|-------------------|-------------------|-------------------|-------------------|------------------|-------------------|-------------------|-------------------|
|                     | $\nu_1(a_1)$      | $\nu_2(e)$        | $\nu_3(t_1)$      | $\nu_4(t_2)$      | $\nu_1(a_1')$     | $\nu_2(a_1'')$   | $\nu_3(e)$        | $\nu_4(e)$        | $\sigma_g$        |
| MPW1K               | 3112              | 1599              | 3248              | 1375              | 3205              | 525              | 3397              | 1444              | 4542              |
| MCOMP2              | 3065              | 1578              | 3195              | 1319              | 3162              | 508              | 3350              | 1412              | 4515              |
| MC-QCISD            | 3029              | 1548              | 3150              | 1326              | 3116              | 555              | 3297              | 1401              | 4358              |
| MCG3                | 3029              | 1559              | 3146              | 1341              | 3111              | 553              | 3291              | 1412              | 4383              |
| MCG3-CHO-SGP        | 3043              | 1566              | 3164              | 1343              | 3124              | 534              | 3305              | 1412              | 4401              |
| MCG2                | 3003              | 1560              | 3122              | 1337              | 3083              | 510              | 3266              | 1396              | 4378              |
| MPW60               | 3158              | 1626              | 3298              | 1400              | 3253              | 523              | 3448              | 1471              | 4590              |
| MCOMP2-SRP          | 3057              | 1544              | 3183              | 1314              | 3147              | 511              | 3334              | 1409              | 4501              |
| MC-QCISD-SRP        | 2997              | 1517              | 3128              | 1293              | 3090              | 585              | 3276              | 1376              | 4322              |
| MCG3-SRP            | 3040              | 1562              | 3163              | 1337              | 3117              | 539              | 3299              | 1406              | 4400              |
| BH&HLYP/6-311G(d,p) | 3107              | 1609              | 3217              | 1389              | 3187              | 500              | 3370              | 1453              | 4518              |
| QCISD/6-311G(d,p)   | 3047              | 1573              | 3167              | 1367              | 3128              | 432              | 3310              | 1436              | 4422              |
| CCSD(T)/cc-VQZ      | 3037              | 1592              | 3153              | 1366              | 3125              | 492              | 3307              | 1445              | 4409              |
| Experiment          | 3026 <sup>a</sup> | 1583 <sup>a</sup> | 3157 <sup>a</sup> | 1367 <sup>a</sup> | 3004 <sup>b</sup> | 606 <sup>b</sup> | 3171 <sup>b</sup> | 1403 <sup>b</sup> | 4401 <sup>c</sup> |

<sup>a</sup>Gray and Robiette (1979), Ref. 36<sup>b</sup>Latest NIST WebBook, Ref. 51<sup>c</sup>JANAF Table, Ref. 35

Table 6. Rate constants ( $\text{cm}^3\text{molecule}^{-1}\text{s}^{-1}$ ) for four SRP surfaces with a classical barrier height of 14.8 kcal/mol

| T(K) | MPW60    |          |          | MCOMP2-SRP |          |          | MC-QCISD-SRP |          |          | MCG3-SRP |          |          | exp. <sup>a</sup> |
|------|----------|----------|----------|------------|----------|----------|--------------|----------|----------|----------|----------|----------|-------------------|
|      | TST      | CVT      | CVT/SCT  | TST        | CVT      | CVT/SCT  | TST          | CVT      | CVT/SCT  | TST      | CVT      | CVT/SCT  |                   |
| 250  | 1.8(-22) | 1.3(-22) | 7.1(-21) | 2.5(-22)   | 1.4(-22) | 1.4(-20) | 1.6(-22)     | 1.0(-22) | 4.9(-21) | 2.7(-22) | 1.8(-22) | 7.4(-21) | n.a. <sup>b</sup> |
| 298  | 1.3(-20) | 1.0(-20) | 1.4(-19) | 1.8(-20)   | 1.2(-20) | 2.4(-19) | 1.3(-20)     | 8.7(-21) | 1.1(-19) | 1.9(-20) | 1.4(-20) | 1.6(-19) | n.a.              |
| 300  | 1.6(-20) | 1.2(-20) | 1.6(-19) | 2.1(-20)   | 1.3(-20) | 2.7(-19) | 1.5(-20)     | 1.0(-20) | 1.3(-19) | 2.2(-20) | 1.6(-20) | 1.8(-19) | n.a.              |
| 348  | 3.4(-19) | 2.8(-19) | 1.7(-18) | 4.6(-19)   | 3.1(-19) | 2.7(-18) | 3.4(-19)     | 2.5(-19) | 1.5(-18) | 4.7(-19) | 3.7(-19) | 2.0(-18) | 2.3(-18)          |
| 400  | 4.3(-18) | 3.6(-18) | 1.4(-17) | 5.7(-18)   | 4.1(-18) | 2.0(-17) | 4.4(-18)     | 3.4(-18) | 1.3(-17) | 5.9(-18) | 4.7(-18) | 1.6(-17) | 1.8(-17)          |
| 600  | 1.4(-15) | 1.3(-15) | 2.3(-15) | 1.9(-15)   | 1.5(-15) | 3.0(-15) | 1.6(-15)     | 1.4(-15) | 2.4(-15) | 1.9(-15) | 1.7(-15) | 2.8(-15) | 2.6(-15)          |
| 700  | 8.0(-15) | 7.5(-15) | 1.1(-14) | 1.1(-14)   | 9.0(-15) | 1.5(-14) | 9.4(-15)     | 8.5(-15) | 1.2(-14) | 1.0(-14) | 9.6(-15) | 1.4(-14) | 1.2(-14)          |
| 800  | 3.0(-14) | 2.9(-14) | 3.8(-14) | 4.0(-14)   | 3.5(-14) | 5.0(-14) | 3.6(-14)     | 3.4(-14) | 4.5(-14) | 3.9(-14) | 3.7(-14) | 4.8(-14) | 4.0(-14)          |
| 900  | 8.8(-14) | 8.4(-14) | 1.0(-13) | 1.2(-13)   | 1.0(-13) | 1.4(-13) | 1.1(-13)     | 1.0(-13) | 1.2(-13) | 1.1(-13) | 1.1(-13) | 1.3(-13) | 1.1(-13)          |
| 1000 | 2.1(-13) | 2.0(-13) | 2.4(-13) | 2.8(-13)   | 2.5(-13) | 3.1(-13) | 2.6(-13)     | 2.5(-13) | 2.9(-13) | 2.7(-13) | 2.6(-13) | 3.0(-13) | 2.4(-13)          |
| 1100 | 4.3(-13) | 4.2(-13) | 4.9(-13) | 5.8(-13)   | 5.3(-13) | 6.3(-13) | 5.5(-13)     | 5.2(-13) | 6.0(-13) | 5.6(-13) | 5.4(-13) | 6.2(-13) | 4.9(-13)          |
| 1250 | 1.1(-12) | 1.0(-12) | 1.2(-12) | 1.4(-12)   | 1.3(-12) | 1.5(-12) | 1.4(-12)     | 1.3(-12) | 1.5(-12) | 1.4(-12) | 1.3(-12) | 1.5(-12) | 1.2(-12)          |
| 1500 | 3.4(-12) | 3.3(-12) | 3.6(-12) | 4.6(-12)   | 4.3(-12) | 4.7(-12) | 4.4(-12)     | 4.3(-12) | 4.6(-12) | 4.4(-12) | 4.3(-12) | 4.6(-12) | 3.8(-12)          |
| 1600 | 5.0(-12) | 4.9(-12) | 5.2(-12) | 6.7(-12)   | 6.2(-12) | 6.7(-12) | 6.5(-12)     | 6.3(-12) | 6.7(-12) | 6.5(-12) | 6.3(-12) | 6.6(-12) | 5.6(-12)          |
| 1700 | 7.0(-12) | 6.9(-12) | 7.2(-12) | 9.4(-12)   | 8.8(-12) | 9.4(-12) | 9.1(-12)     | 9.0(-12) | 9.3(-12) | 9.1(-12) | 8.8(-12) | 9.3(-12) | 8.0(-12)          |
| 1800 | 9.5(-12) | 9.3(-12) | 9.7(-12) | 1.3(-11)   | 1.2(-11) | 1.3(-11) | 1.2(-11)     | 1.2(-11) | 1.3(-11) | 1.2(-11) | 1.2(-11) | 1.3(-11) | 1.1(-11)          |
| 1900 | 1.3(-11) | 1.2(-11) | 1.3(-11) | 1.7(-11)   | 1.6(-11) | 1.7(-11) | 1.7(-11)     | 1.6(-11) | 1.7(-11) | 1.6(-11) | 1.6(-11) | 1.7(-11) | 1.5(-11)          |
| 1950 | 1.4(-11) | 1.4(-11) | 1.5(-11) | 1.9(-11)   | 1.8(-11) | 1.9(-11) | 1.9(-11)     | 1.9(-11) | 1.9(-11) | 1.9(-11) | 1.8(-11) | 1.9(-11) | 1.7(-11)          |
| 2000 | 1.6(-11) | 1.6(-11) | 1.6(-11) | 2.2(-11)   | 2.0(-11) | 2.2(-11) | 2.1(-11)     | 2.1(-11) | 2.2(-11) | 2.1(-11) | 2.1(-11) | 2.1(-11) | n.a.              |
| 2400 | 3.8(-11) | 3.7(-11) | 3.7(-11) | 5.1(-11)   | 4.8(-11) | 5.0(-11) | 5.0(-11)     | 4.9(-11) | 5.0(-11) | 4.9(-11) | 4.8(-11) | 4.9(-11) | n.a.              |

<sup>a</sup>from Ref. 10.<sup>b</sup>n.a. denotes not available

Table 7.  $k^{\text{CVT}}/k^{\text{TST}}$  and  $k^{\text{CVT/SCT}}/k^{\text{CVT}}$  on four SRP surfaces

| T(K) | $k^{\text{CVT}}/k^{\text{TST}}$ |            |              |          | $k^{\text{CVT/SCT}}/k^{\text{CVT}}$ |            |              |          |
|------|---------------------------------|------------|--------------|----------|-------------------------------------|------------|--------------|----------|
|      | MPW60                           | MCOMP2-SRP | MC-QCISD-SRP | MCG3-SRP | MPW60                               | MCOMP2-SRP | MC-QCISD-SRP | MCG3-SRP |
| 250  | 0.71                            | 0.58       | 0.63         | 0.68     | 55.64                               | 95.10      | 48.29        | 40.61    |
| 300  | 0.76                            | 0.64       | 0.69         | 0.73     | 13.47                               | 20.09      | 12.34        | 10.91    |
| 400  | 0.83                            | 0.73       | 0.77         | 0.81     | 3.84                                | 4.87       | 3.68         | 3.44     |
| 600  | 0.91                            | 0.83       | 0.87         | 0.89     | 1.74                                | 1.94       | 1.71         | 1.67     |
| 1000 | 0.96                            | 0.90       | 0.95         | 0.95     | 1.19                                | 1.25       | 1.18         | 1.18     |
| 1500 | 0.98                            | 0.93       | 0.98         | 0.97     | 1.07                                | 1.10       | 1.06         | 1.07     |
| 2400 | 0.99                            | 0.94       | 0.99         | 0.98     | 1.02                                | 1.04       | 1.01         | 1.02     |

Table 8. Arrhenius activation energies (in kcal/mol) over various temperature ranges (in K).

|                         | 250 – 295         | 295 – 305 | 348 – 800 | 800 – 1950 | 1950 – 2400 |
|-------------------------|-------------------|-----------|-----------|------------|-------------|
| MPW1K                   | 8.8               | 9.4       | 11.3      | 14.8       | 18.5        |
| MCOMP2-v2m-GP           | 9.5               | 10.3      | 12.8      | 16.7       | 20.5        |
| MC-QCISD-v2m-GP         | 9.3               | 10.0      | 12.6      | 16.6       | 20.4        |
| MCG3-CHO-SGP            | 9.0               | 10.0      | 12.5      | 16.3       | 20.2        |
| MPW60                   | 9.2               | 9.9       | 12.2      | 16.0       | 19.8        |
| MCOMP2-SRP              | 8.8               | 9.5       | 12.0      | 16.0       | 19.8        |
| MC-QCISD-SRP            | 9.6               | 10.3      | 12.6      | 16.3       | 20.1        |
| MCG3-SRP                | 9.4               | 10.1      | 12.3      | 16.1       | 19.9        |
| Experiment <sup>a</sup> | n.a. <sup>b</sup> | n.a.      | 11.8      | 16.3       | n.a.        |

<sup>a</sup>Calculated from the rate constant expression in Ref. 10.

<sup>b</sup>n.a. denotes not available

**Figure Captions**

Figure 1  $V_{\text{MEP}}$  for four proposed SRP surfaces as a function of reaction coordinate  $s$ .

Figure 2  $V_a^G$  for four proposed SRP surfaces as a function of reaction coordinate  $s$ .

Figure 3 Arrhenius plot of CVT/SCT rate constants calculated from four proposed SRP surfaces compared with experimental results.

Figure 1

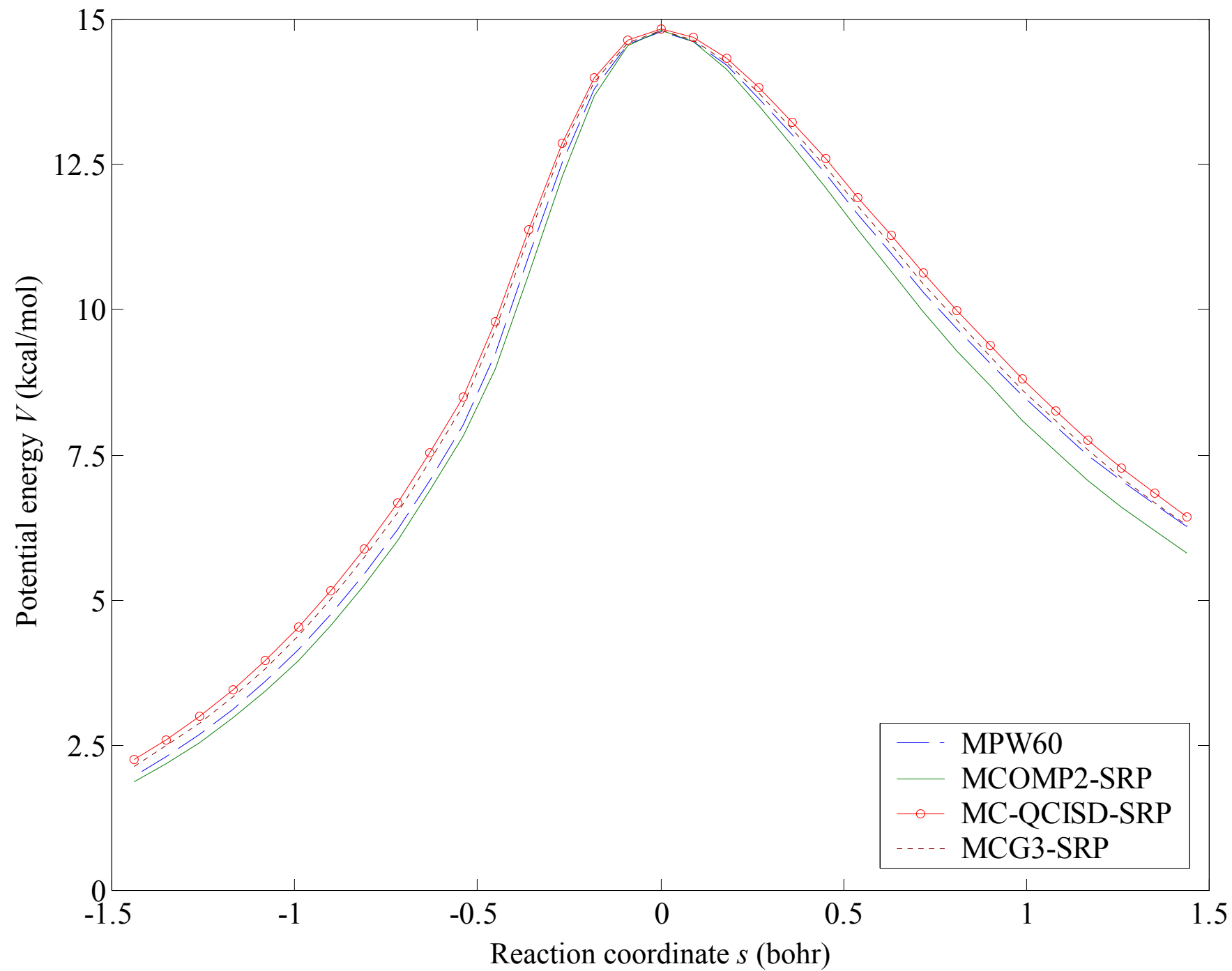


Figure 2

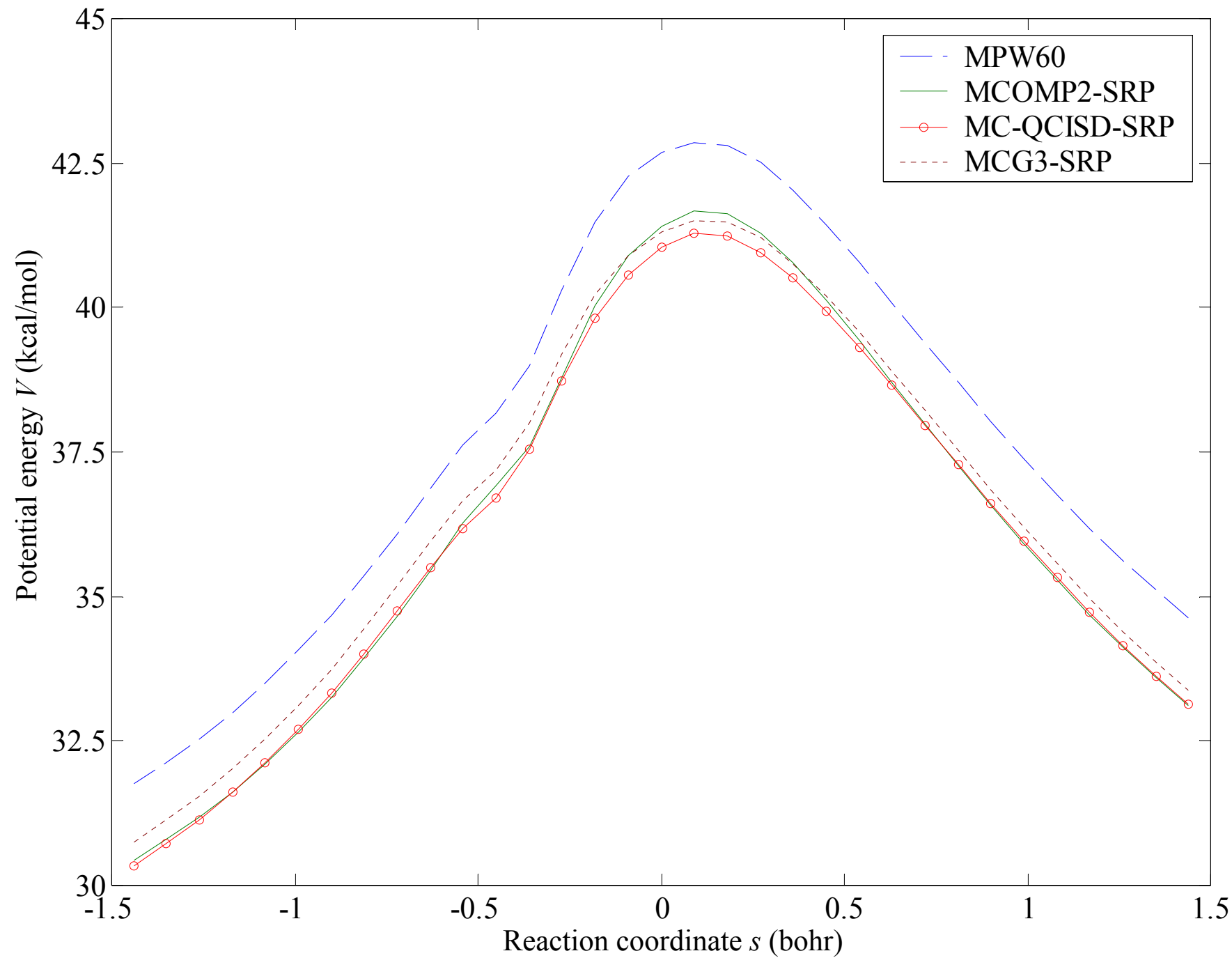
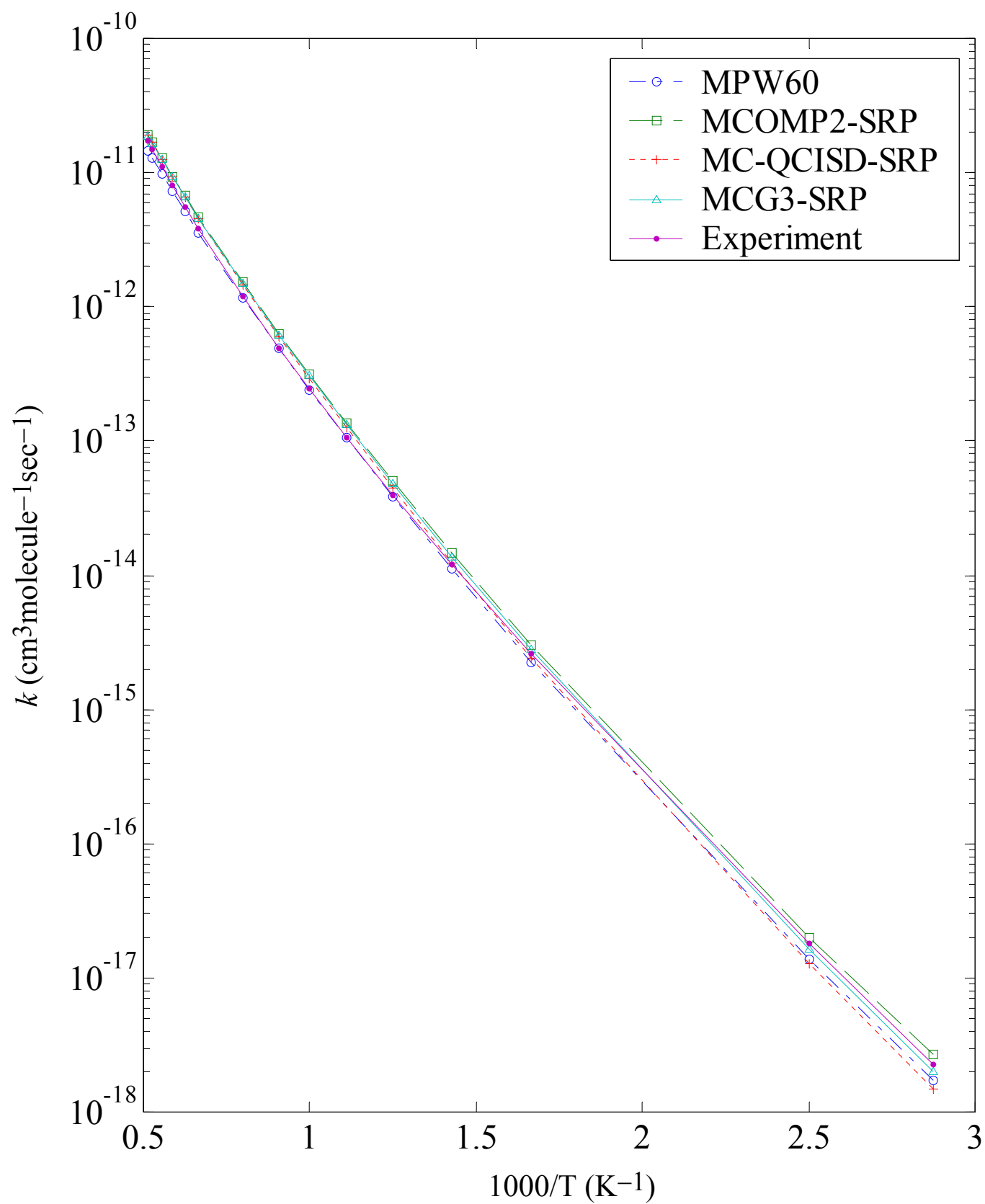


Figure 3



**Supporting information for****A Parameterized Direct Dynamics Study of the Reaction of H with CH<sub>4</sub>: Rate Constants from 250 to 2400 K**

Jingzhi Pu and Donald G. Truhlar

*Department of Chemistry and Supercomputer Institute, University of Minnesota, Minneapolis, MN 55455-0431*

In this supporting information, we present additional dynamics calculations for standard methods, for preliminary parameterized SRP methods, and for our best SRP methods with modified parameterizations. To differentiate the further parameterized SRP surfaces from the four SRP methods present in the text, we label the methods as follows:

- (1) for MPW $X$  series,  $X$  denotes the percentage of HF exchange.
- (2) for MCCM-SRP methods with a barrier height other than 14.8 kcal/mol, we add a two-number suffix "- $Y$ - $Z$ " to declare the barrier height and the reaction energy explicitly in each method, where  $Y$  denotes the barrier height and  $Z$  denotes the reaction energy. For example, MCOMP2-SRP-15.1-3.3 denotes an SRP method based on MCOMP2 with a barrier height of 15.1 kcal/mol and a reaction energy of 3.3 kcal/mol. The parameterizations of these SRP surfaces follow the procedures described in the text.

Table 1-S: presents reaction rate constants for the four standard electronic structure PESs from which the four proposed SRP surfaces derive. These are MPW1K, MCOMP2, MC-QCISD, and MCG3-CHO-SGP.

Table 2-S: presents rate constants for our best methods with further adjustments of SRP, including MPW60, MCOMP2-15.1-3.3, MC-QCISD-14.8-3.3, and MCG3-15.1-3.3. Note that the MC-QCISD-14.8-3.3 is identical to the MC-QCISD-SRP in the text.

Table 3-S~5-S: gives rate constants for a series of MPW $X$  methods with the percentage of HF exchange varied from 57 to 59. The results for MC-QCISD-SRP- $Y$ - $Z$  methods with the same barrier height as each MPW $X$  surface are presented for comparison.

Table 6-S: presents rate constants on the MPW60 surface with all frequencies scaled by 0.96 in calculations of  $V_a^G$ , vibrational partition functions, and effective mass in SCT.

Table 1-S. Rate constants ( $\text{cm}^3\text{molecule}^{-1}\text{s}^{-1}$ ) for standard methods: MPW1K, MCOMP2, MC-QCISD, and MCG3-CHO-SGP.

| T(K) | MPW1K    |          |          | MCOMP2   |          |          | MC-QCISD |          |          | MCG3-CHO-SGP |          |          | exp. <sup>a</sup> |
|------|----------|----------|----------|----------|----------|----------|----------|----------|----------|--------------|----------|----------|-------------------|
|      | TST      | CVT      | CVT/SCT  | TST      | CVT      | CVT/SCT  | TST      | CVT      | CVT/SCT  | TST          | CVT      | CVT/SCT  |                   |
| 250  | 2.6(-21) | 1.9(-21) | 4.4(-20) | 4.8(-23) | 2.8(-23) | 2.7(-21) | 7.3(-23) | 4.9(-23) | 4.7(-23) | 1.5(-22)     | 1.1(-22) | 5.2(-21) | n.a. <sup>b</sup> |
| 298  | 1.3(-19) | 9.7(-20) | 7.7(-19) | 4.5(-21) | 2.9(-21) | 6.0(-20) | 6.4(-21) | 4.6(-21) | 9.5(-20) | 1.2(-20)     | 8.8(-21) | 1.1(-19) | n.a.              |
| 300  | 1.5(-19) | 1.1(-19) | 8.6(-19) | 5.3(-21) | 3.4(-21) | 6.7(-20) | 7.5(-21) | 5.4(-21) | 1.1(-19) | 1.4(-20)     | 1.0(-20) | 1.3(-19) | n.a.              |
| 348  | 2.4(-18) | 1.9(-18) | 8.2(-18) | 1.4(-19) | 9.5(-20) | 8.0(-19) | 1.9(-19) | 1.4(-19) | 1.2(-18) | 3.1(-19)     | 2.5(-19) | 1.5(-18) | 2.3(-18)          |
| 400  | 2.4(-17) | 2.0(-17) | 5.7(-17) | 2.0(-18) | 1.5(-18) | 7.0(-18) | 2.6(-18) | 2.1(-18) | 9.8(-18) | 4.1(-18)     | 3.3(-18) | 1.2(-17) | 1.8(-17)          |
| 600  | 4.5(-15) | 4.1(-15) | 6.3(-15) | 9.0(-16) | 7.6(-16) | 1.4(-15) | 1.1(-15) | 9.7(-16) | 1.8(-15) | 1.5(-15)     | 1.3(-15) | 2.2(-15) | 2.6(-15)          |
| 700  | 2.2(-14) | 2.0(-14) | 2.7(-14) | 5.5(-15) | 4.8(-15) | 7.7(-15) | 6.7(-15) | 6.0(-15) | 9.6(-15) | 8.5(-15)     | 7.8(-15) | 1.1(-14) | 1.2(-14)          |
| 800  | 7.2(-14) | 6.9(-14) | 8.6(-14) | 2.2(-14) | 2.0(-14) | 2.8(-14) | 2.7(-14) | 2.5(-14) | 3.5(-14) | 3.3(-14)     | 3.1(-14) | 4.1(-14) | 4.0(-14)          |
| 900  | 1.9(-13) | 1.8(-13) | 2.2(-13) | 6.9(-14) | 6.2(-14) | 8.2(-14) | 8.0(-14) | 7.5(-14) | 9.8(-14) | 9.6(-14)     | 9.1(-14) | 1.1(-13) | 1.1(-13)          |
| 1000 | 4.2(-13) | 4.1(-13) | 4.7(-13) | 1.7(-13) | 1.6(-13) | 2.0(-13) | 2.0(-13) | 1.9(-13) | 2.3(-13) | 2.3(-12)     | 2.2(-12) | 2.7(-12) | 2.4(-13)          |
| 1100 | 8.3(-13) | 8.1(-13) | 8.9(-13) | 3.7(-13) | 3.4(-13) | 4.1(-13) | 4.3(-13) | 4.1(-13) | 4.8(-13) | 4.9(-12)     | 4.7(-12) | 5.4(-12) | 4.9(-13)          |
| 1250 | 1.9(-12) | 1.9(-12) | 2.0(-12) | 9.5(-13) | 8.9(-13) | 1.0(-12) | 1.1(-12) | 1.0(-12) | 1.2(-12) | 1.2(-12)     | 1.2(-12) | 1.3(-12) | 1.2(-12)          |
| 1500 | 5.5(-12) | 5.5(-12) | 5.7(-12) | 3.2(-12) | 3.0(-12) | 3.3(-12) | 3.6(-12) | 3.5(-12) | 3.8(-12) | 4.0(-12)     | 3.9(-12) | 4.2(-12) | 3.8(-12)          |
| 1600 | 7.8(-12) | 7.7(-12) | 8.0(-12) | 4.7(-12) | 4.5(-12) | 4.8(-12) | 5.4(-12) | 5.2(-12) | 5.6(-12) | 5.9(-12)     | 5.7(-12) | 6.1(-12) | 5.6(-12)          |
| 1700 | 1.1(-11) | 1.1(-11) | 1.1(-11) | 6.7(-12) | 6.4(-12) | 6.8(-12) | 7.6(-12) | 7.4(-12) | 7.9(-12) | 8.3(-12)     | 8.1(-12) | 8.5(-12) | 8.0(-12)          |
| 1800 | 1.4(-11) | 1.4(-11) | 1.4(-11) | 9.2(-12) | 8.8(-12) | 9.3(-12) | 1.0(-11) | 1.0(-11) | 1.1(-11) | 1.1(-11)     | 1.1(-11) | 1.2(-11) | 1.1(-11)          |
| 1900 | 1.8(-11) | 1.8(-11) | 1.9(-11) | 1.2(-11) | 1.2(-11) | 1.2(-11) | 1.4(-11) | 1.4(-11) | 1.4(-11) | 1.5(-11)     | 1.5(-11) | 1.5(-11) | 1.5(-11)          |
| 1950 | 2.1(-11) | 2.1(-11) | 2.1(-11) | 1.4(-11) | 1.3(-11) | 1.4(-11) | 1.6(-11) | 1.5(-11) | 1.6(-11) | 1.7(-11)     | 1.7(-11) | 1.7(-11) | 1.7(-11)          |
| 2000 | 2.3(-11) | 2.3(-11) | 2.4(-11) | 1.6(-11) | 1.5(-11) | 1.6(-11) | 1.8(-11) | 1.8(-11) | 1.8(-11) | 2.0(-11)     | 1.9(-11) | 2.0(-11) | n.a.              |
| 2400 | 5.1(-11) | 5.1(-11) | 5.1(-11) | 3.9(-11) | 3.7(-11) | 3.8(-11) | 4.4(-11) | 4.2(-11) | 4.4(-11) | 4.6(-11)     | 4.5(-11) | 4.6(-11) | n.a.              |

<sup>a</sup>from Ref. 8<sup>b</sup>n.a. denotes not available

Table 2-S. Rate constants ( $\text{cm}^3\text{molecule}^{-1}\text{s}^{-1}$ ) for our best SRP surfaces with further parameterizations.

| T(K) | MPW58    |          |          | MCOMP2-SRP-15.1-3.3 |          |          | MC-QCISD-SRP-14.8-3.3 |          |          | MCG3-SRP-15.1-3.3 |          |          | exp. <sup>a</sup> |
|------|----------|----------|----------|---------------------|----------|----------|-----------------------|----------|----------|-------------------|----------|----------|-------------------|
|      | TST      | CVT      | CVT/SCT  | TST                 | CVT      | CVT/SCT  | TST                   | CVT      | CVT/SCT  | TST               | CVT      | CVT/SCT  |                   |
| 250  | 2.4(-22) | 1.7(-22) | 8.6(-21) | 1.3(-22)            | 7.8(-23) | 9.5(-21) | 1.6(-22)              | 1.0(-22) | 4.9(-21) | 1.5(-22)          | 1.0(-22) | 4.7(-21) | n.a. <sup>b</sup> |
| 298  | 1.7(-20) | 1.3(-20) | 1.7(-19) | 1.0(-22)            | 6.8(-21) | 1.7(-19) | 1.3(-20)              | 8.7(-21) | 1.1(-19) | 1.2(-20)          | 8.7(-21) | 1.1(-19) | n.a.              |
| 300  | 2.0(-20) | 1.5(-20) | 1.9(-19) | 1.2(-20)            | 8.0(-21) | 1.9(-19) | 1.5(-20)              | 1.0(-20) | 1.3(-19) | 1.4(-20)          | 1.0(-20) | 1.2(-19) | n.a.              |
| 348  | 4.3(-20) | 3.4(-19) | 2.0(-18) | 2.8(-19)            | 2.0(-19) | 1.9(-18) | 3.4(-19)              | 2.5(-19) | 1.5(-18) | 3.2(-19)          | 2.5(-19) | 1.4(-18) | 2.3(-18)          |
| 400  | 5.3(-18) | 4.4(-18) | 1.6(-17) | 3.7(-18)            | 2.8(-18) | 1.5(-17) | 4.4(-17)              | 3.4(-18) | 1.3(-17) | 4.1(-18)          | 3.3(-19) | 1.2(-17) | 1.8(-17)          |
| 600  | 1.6(-15) | 1.5(-15) | 2.5(-15) | 1.4(-15)            | 1.1(-15) | 2.3(-15) | 1.6(-15)              | 1.4(-15) | 2.4(-15) | 1.5(-15)          | 1.3(-15) | 2.2(-15) | 2.6(-15)          |
| 700  | 9.0(-15) | 8.3(-15) | 1.2(-14) | 7.9(-15)            | 6.9(-15) | 1.1(-14) | 9.4(-15)              | 8.5(-15) | 1.2(-14) | 8.5(-15)          | 7.8(-15) | 1.1(-14) | 1.2(-14)          |
| 800  | 3.3(-14) | 3.2(-14) | 4.2(-14) | 3.1(-14)            | 2.7(-14) | 4.0(-14) | 3.6(-14)              | 3.4(-14) | 4.5(-14) | 3.3(-14)          | 3.1(-14) | 4.1(-14) | 4.0(-14)          |
| 900  | 9.5(-14) | 9.1(-14) | 1.1(-13) | 9.1(-14)            | 8.2(-14) | 1.1(-13) | 1.1(-13)              | 1.0(-13) | 1.2(-13) | 9.7(-14)          | 9.2(-14) | 1.1(-13) | 1.1(-13)          |
| 1000 | 2.3(-13) | 2.2(-13) | 2.6(-13) | 2.6(-13)            | 2.5(-13) | 2.9(-13) | 2.6(-13)              | 2.5(-13) | 2.9(-13) | 2.4(-13)          | 2.2(-13) | 2.7(-13) | 2.4(-13)          |
| 1100 | 4.7(-13) | 4.5(-13) | 5.2(-13) | 4.7(-13)            | 4.3(-13) | 5.2(-13) | 5.5(-13)              | 5.2(-13) | 6.0(-13) | 5.0(-13)          | 4.8(-13) | 5.4(-13) | 4.9(-13)          |
| 1250 | 1.1(-12) | 1.1(-12) | 1.2(-12) | 1.2(-13)            | 1.1(-12) | 1.3(-13) | 1.4(-12)              | 1.3(-12) | 1.5(-12) | 1.2(-12)          | 1.2(-12) | 1.3(-12) | 1.2(-12)          |
| 1500 | 3.6(-12) | 3.5(-12) | 3.8(-12) | 3.8(-12)            | 3.6(-12) | 4.0(-12) | 4.4(-12)              | 4.3(-12) | 4.6(-12) | 4.0(-12)          | 3.9(-12) | 4.2(-12) | 3.8(-12)          |
| 1600 | 5.2(-12) | 5.1(-12) | 5.4(-12) | 5.6(-12)            | 5.3(-12) | 5.8(-12) | 6.5(-12)              | 6.3(-12) | 6.7(-12) | 5.9(-12)          | 5.8(-12) | 6.1(-12) | 5.6(-12)          |
| 1700 | 7.3(-12) | 7.2(-12) | 7.5(-12) | 8.0(-12)            | 7.5(-12) | 8.1(-12) | 9.1(-12)              | 9.0(-12) | 9.3(-12) | 8.3(-12)          | 8.1(-12) | 8.5(-12) | 8.0(-12)          |
| 1800 | 9.9(-12) | 9.8(-12) | 1.0(-11) | 1.1(-11)            | 1.0(-11) | 1.1(-11) | 1.2(-11)              | 1.2(-11) | 1.3(-11) | 1.1(-11)          | 1.1(-11) | 1.2(-11) | 1.1(-11)          |
| 1900 | 1.3(-11) | 1.3(-11) | 1.3(-11) | 1.4(-11)            | 1.4(-11) | 1.4(-11) | 1.7(-11)              | 1.6(-11) | 1.7(-11) | 1.5(-11)          | 1.5(-11) | 1.5(-11) | 1.5(-11)          |
| 1950 | 1.5(-11) | 1.5(-11) | 1.5(-11) | 1.7(-11)            | 1.6(-11) | 1.6(-11) | 1.9(-11)              | 1.9(-11) | 1.9(-11) | 1.7(-11)          | 1.7(-11) | 1.8(-11) | 1.7(-11)          |
| 2000 | 1.7(-11) | 1.7(-11) | 1.7(-11) | 1.9(-11)            | 1.8(-11) | 1.9(-11) | 2.1(-11)              | 2.1(-11) | 2.2(-11) | 2.0(-11)          | 1.9(-11) | 2.0(-11) | n.a.              |
| 2400 | 3.9(-11) | 3.9(-11) | 3.9(-11) | 4.4(-11)            | 4.2(-11) | 4.3(-11) | 5.0(-11)              | 4.9(-11) | 5.0(-11) | 4.6(-11)          | 4.5(-11) | 4.6(-11) | n.a.              |

<sup>a</sup>from Ref. 10.<sup>b</sup>n.a. denotes not available

Table 3-S. Rate constants ( $\text{cm}^3 \text{molecule}^{-1} \text{s}^{-1}$ ) for MPW57 and MC-QCISD-SRP-14.5-3.3; both surfaces have a barrier height of 14.5 kcal/mol.

| T(K) | MPW57    |          |          | MC-QCISD-SRP-14.5-3.3 |          |          | exp. <sup>a</sup> |
|------|----------|----------|----------|-----------------------|----------|----------|-------------------|
|      | TST      | CVT      | CVT/SCT  | TST                   | CVT      | CVT/SCT  |                   |
| 250  | 2.8(-22) | 2.0(-22) | 9.5(-21) | 2.8(-22)              | 1.8(-22) | 7.3(-21) | n.a. <sup>b</sup> |
| 298  | 2.0(-20) | 1.5(-20) | 1.9(-19) | 2.0(-20)              | 1.4(-20) | 1.6(-19) | n.a.              |
| 300  | 2.3(-20) | 1.7(-20) | 2.1(-19) | 2.3(-20)              | 1.6(-20) | 1.8(-19) | n.a.              |
| 348  | 4.8(-19) | 3.8(-19) | 2.2(-18) | 5.0(-19)              | 3.7(-19) | 2.1(-18) | 2.3(-18)          |
| 400  | 5.8(-18) | 4.8(-18) | 1.7(-17) | 6.3(-18)              | 4.9(-18) | 1.7(-17) | 1.8(-17)          |
| 600  | 1.7(-15) | 1.6(-15) | 2.7(-15) | 2.1(-15)              | 1.8(-15) | 3.0(-15) | 2.6(-15)          |
| 700  | 9.5(-15) | 8.8(-15) | 1.3(-14) | 1.2(-14)              | 1.0(-14) | 1.5(-14) | 1.2(-14)          |
| 800  | 3.5(-14) | 3.3(-14) | 4.4(-14) | 4.4(-14)              | 4.0(-14) | 5.3(-14) | 4.0(-14)          |
| 900  | 1.0(-13) | 9.6(-14) | 1.2(-13) | 1.3(-13)              | 1.2(-13) | 1.5(-13) | 1.1(-13)          |
| 1000 | 2.4(-13) | 2.3(-13) | 2.7(-13) | 3.0(-13)              | 2.9(-13) | 3.4(-13) | 2.4(-13)          |
| 1100 | 4.8(-13) | 4.7(-13) | 5.4(-13) | 6.3(-13)              | 6.1(-13) | 6.9(-13) | 4.9(-13)          |
| 1250 | 1.2(-12) | 1.2(-12) | 1.3(-12) | 1.6(-12)              | 1.5(-12) | 1.7(-12) | 1.2(-12)          |
| 1500 | 3.7(-12) | 3.6(-12) | 3.9(-12) | 4.9(-12)              | 4.8(-12) | 5.1(-12) | 3.8(-12)          |
| 1600 | 5.4(-12) | 5.3(-12) | 5.6(-12) | 7.2(-12)              | 7.1(-12) | 7.4(-12) | 5.6(-12)          |
| 1700 | 7.5(-12) | 7.4(-12) | 7.7(-12) | 1.0(-11)              | 9.9(-12) | 1.0(-11) | 8.0(-12)          |
| 1800 | 1.0(-11) | 1.0(-11) | 1.0(-11) | 1.4(-11)              | 1.3(-11) | 1.4(-11) | 1.1(-11)          |
| 1900 | 1.3(-11) | 1.3(-11) | 1.4(-11) | 1.8(-11)              | 1.8(-11) | 1.8(-11) | 1.5(-11)          |
| 1950 | 1.5(-11) | 1.5(-11) | 1.5(-11) | 2.1(-11)              | 2.0(-11) | 2.1(-11) | 1.7(-11)          |
| 2000 | 1.7(-11) | 1.7(-11) | 1.8(-11) | 2.3(-11)              | 2.3(-11) | 2.4(-11) | n.a.              |
| 2400 | 4.0(-11) | 3.9(-11) | 4.0(-11) | 5.4(-11)              | 5.4(-11) | 5.4(-11) | n.a.              |

<sup>a</sup>from Ref. 8.

<sup>b</sup>n.a. denotes not available

Table 4-S. Rate constants ( $\text{cm}^3 \text{molecule}^{-1} \text{s}^{-1}$ ) for MPW58 and MC-QCISD-SRP-14.6-3.3; both surfaces have a barrier height of 14.6 kcal/mol.

| T(K) | MPW58    |          |          | MC-QCISD-SRP-14.6-3.3 |          |          | exp. <sup>a</sup> |
|------|----------|----------|----------|-----------------------|----------|----------|-------------------|
|      | TST      | CVT      | CVT/SCT  | TST                   | CVT      | CVT/SCT  |                   |
| 250  | 2.4(-22) | 1.7(-22) | 8.6(-21) | 2.3(-22)              | 1.5(-22) | 6.4(-21) | n.a. <sup>b</sup> |
| 298  | 1.7(-20) | 1.3(-20) | 1.7(-19) | 1.7(-20)              | 1.2(-20) | 1.4(-19) | n.a.              |
| 300  | 2.0(-20) | 1.5(-20) | 1.9(-19) | 2.0(-20)              | 1.4(-20) | 1.6(-19) | n.a.              |
| 348  | 4.3(-20) | 3.4(-19) | 2.0(-18) | 4.4(-19)              | 3.2(-19) | 1.8(-18) | 2.3(-18)          |
| 400  | 5.3(-18) | 4.4(-18) | 1.6(-17) | 5.6(-18)              | 4.3(-18) | 1.5(-17) | 1.8(-17)          |
| 600  | 1.6(-15) | 1.5(-15) | 2.5(-15) | 1.9(-15)              | 1.7(-15) | 2.8(-15) | 2.6(-15)          |
| 700  | 9.0(-15) | 8.3(-15) | 1.2(-14) | 1.1(-14)              | 9.7(-15) | 1.4(-14) | 1.2(-14)          |
| 800  | 3.3(-14) | 3.2(-14) | 4.2(-14) | 4.1(-14)              | 3.8(-14) | 5.0(-14) | 4.0(-14)          |
| 900  | 9.5(-14) | 9.1(-14) | 1.1(-13) | 1.2(-13)              | 1.1(-13) | 1.4(-13) | 1.1(-13)          |
| 1000 | 2.3(-13) | 2.2(-13) | 2.6(-13) | 2.9(-13)              | 2.7(-13) | 3.2(-13) | 2.4(-13)          |
| 1100 | 4.7(-13) | 4.5(-13) | 5.2(-13) | 6.0(-13)              | 5.8(-13) | 6.6(-13) | 4.9(-13)          |
| 1250 | 1.1(-12) | 1.1(-12) | 1.2(-12) | 1.5(-12)              | 1.4(-12) | 1.6(-12) | 1.2(-12)          |
| 1500 | 3.6(-12) | 3.5(-12) | 3.8(-12) | 4.8(-12)              | 4.7(-12) | 4.9(-12) | 3.8(-12)          |
| 1600 | 5.2(-12) | 5.1(-12) | 5.4(-12) | 7.0(-12)              | 6.8(-12) | 7.1(-12) | 5.6(-12)          |
| 1700 | 7.3(-12) | 7.2(-12) | 7.5(-12) | 9.8(-12)              | 9.6(-12) | 9.9(-12) | 8.0(-12)          |
| 1800 | 9.9(-12) | 9.8(-12) | 1.0(-11) | 1.3(-11)              | 1.3(-11) | 1.3(-11) | 1.1(-11)          |
| 1900 | 1.3(-11) | 1.3(-11) | 1.3(-11) | 1.8(-11)              | 1.7(-11) | 1.8(-11) | 1.5(-11)          |
| 1950 | 1.5(-11) | 1.5(-11) | 1.5(-11) | 2.0(-11)              | 2.0(-11) | 2.0(-11) | 1.7(-11)          |
| 2000 | 1.7(-11) | 1.7(-11) | 1.7(-11) | 2.3(-11)              | 2.2(-11) | 2.3(-11) | n.a.              |
| 2400 | 3.9(-11) | 3.9(-11) | 3.9(-11) | 5.3(-11)              | 5.2(-11) | 5.3(-11) | n.a.              |

<sup>a</sup>from Ref. 8.

<sup>b</sup>n.a. denotes not available

Table 5-S. Rate constants ( $\text{cm}^3 \text{molecule}^{-1} \text{s}^{-1}$ ) for MPW59 and MC-QCISD-SRP-14.7-3.3; both surfaces have a barrier height of 14.7 kcal/mol.

| T(K) | MPW59    |          |          | MC-QCISD-SRP-14.7-3.3 |          |          | exp. <sup>a</sup> |
|------|----------|----------|----------|-----------------------|----------|----------|-------------------|
|      | TST      | CVT      | CVT/SCT  | TST                   | CVT      | CVT/SCT  |                   |
| 250  | 2.1(-22) | 1.5(-22) | 7.8(-21) | 2.0(-22)              | 1.2(-22) | 5.6(-21) | n.a. <sup>b</sup> |
| 298  | 1.5(-20) | 1.2(-20) | 1.6(-19) | 1.5(-20)              | 1.0(-20) | 1.3(-19) | n.a.              |
| 300  | 1.8(-20) | 1.3(-20) | 1.7(-19) | 1.7(-20)              | 1.2(-20) | 1.4(-19) | n.a.              |
| 348  | 3.8(-19) | 3.1(-19) | 1.9(-18) | 3.9(-19)              | 2.8(-19) | 1.7(-18) | 2.3(-18)          |
| 400  | 4.8(-18) | 4.0(-18) | 1.5(-17) | 5.0(-18)              | 3.9(-18) | 1.4(-18) | 1.8(-17)          |
| 600  | 1.5(-15) | 1.4(-15) | 2.4(-15) | 1.7(-15)              | 1.5(-15) | 2.6(-15) | 2.6(-15)          |
| 700  | 8.5(-15) | 7.9(-15) | 1.2(-14) | 1.0(-14)              | 9.1(-15) | 1.3(-14) | 1.2(-14)          |
| 800  | 3.2(-14) | 3.0(-14) | 4.0(-14) | 3.9(-14)              | 3.6(-14) | 4.7(-14) | 4.0(-14)          |
| 900  | 9.1(-14) | 8.7(-14) | 1.1(-13) | 1.1(-13)              | 1.1(-13) | 1.3(-13) | 1.1(-13)          |
| 1000 | 2.2(-13) | 2.1(-13) | 2.5(-13) | 2.7(-13)              | 2.6(-13) | 3.1(-13) | 2.4(-13)          |
| 1100 | 4.5(-13) | 4.4(-13) | 5.0(-13) | 5.7(-13)              | 5.5(-13) | 6.3(-13) | 4.9(-13)          |
| 1250 | 1.1(-12) | 1.1(-12) | 1.2(-12) | 1.4(-12)              | 1.4(-12) | 1.5(-12) | 1.2(-12)          |
| 1500 | 3.5(-12) | 3.4(-12) | 3.7(-12) | 4.6(-12)              | 4.5(-12) | 4.8(-12) | 3.8(-12)          |
| 1600 | 5.1(-12) | 5.0(-12) | 5.3(-12) | 6.7(-12)              | 6.6(-12) | 6.9(-12) | 5.6(-12)          |
| 1700 | 7.1(-12) | 7.0(-12) | 7.4(-12) | 9.4(-12)              | 9.3(-12) | 9.6(-12) | 8.0(-12)          |
| 1800 | 9.7(-12) | 9.6(-12) | 1.0(-11) | 1.3(-11)              | 1.3(-11) | 1.3(-11) | 1.1(-11)          |
| 1900 | 1.3(-11) | 1.3(-11) | 1.3(-11) | 1.7(-11)              | 1.7(-11) | 1.7(-11) | 1.5(-11)          |
| 1950 | 1.5(-11) | 1.4(-11) | 1.5(-11) | 1.9(-11)              | 1.9(-11) | 2.0(-11) | 1.7(-11)          |
| 2000 | 1.6(-11) | 1.6(-11) | 1.7(-11) | 2.2(-11)              | 2.2(-11) | 2.2(-11) | n.a.              |
| 2400 | 3.8(-11) | 3.8(-11) | 3.9(-11) | 5.2(-11)              | 5.1(-11) | 5.2(-11) | n.a.              |

<sup>a</sup>from Ref. 8.

<sup>b</sup>n.a. denotes not available

Table 6-S. Rate constants ( $\text{cm}^3 \text{molecule}^{-1} \text{s}^{-1}$ ) for MPW60 and MPW60 with all frequencies scaled by a factor of 0.96.

| T(K) | MPW60    |          |          | MPW60-FreqScaled-0.96 <sup>a</sup> |          |          | exp. <sup>b</sup> |
|------|----------|----------|----------|------------------------------------|----------|----------|-------------------|
|      | TST      | CVT      | CVT/SCT  | TST                                | CVT      | CVT/SCT  |                   |
| 250  | 1.8(-22) | 1.3(-22) | 7.1(-21) | 1.6(-22)                           | 1.2(-22) | 7.2(-21) | n.a. <sup>c</sup> |
| 298  | 1.3(-20) | 1.0(-20) | 1.4(-19) | 1.2(-20)                           | 9.7(-21) | 1.4(-19) | n.a.              |
| 300  | 1.6(-20) | 1.2(-20) | 1.6(-19) | 1.5(-20)                           | 1.1(-20) | 1.6(-19) | n.a.              |
| 348  | 3.4(-19) | 2.8(-19) | 1.7(-18) | 3.3(-19)                           | 2.7(-19) | 1.8(-18) | 2.3(-18)          |
| 400  | 4.3(-18) | 3.6(-18) | 1.4(-17) | 4.2(-18)                           | 3.6(-18) | 1.4(-17) | 1.8(-17)          |
| 600  | 1.4(-15) | 1.3(-15) | 2.3(-15) | 1.4(-15)                           | 1.3(-15) | 2.3(-15) | 2.6(-15)          |
| 700  | 8.0(-15) | 7.5(-15) | 1.1(-14) | 8.2(-15)                           | 7.7(-15) | 1.2(-14) | 1.2(-14)          |
| 800  | 3.0(-14) | 2.9(-14) | 3.8(-14) | 3.1(-14)                           | 3.0(-14) | 4.0(-14) | 4.0(-14)          |
| 900  | 8.8(-14) | 8.4(-14) | 1.0(-13) | 9.1(-14)                           | 8.7(-14) | 1.1(-13) | 1.1(-13)          |
| 1000 | 2.1(-13) | 2.0(-13) | 2.4(-13) | 2.2(-13)                           | 2.1(-13) | 2.5(-13) | 2.4(-13)          |
| 1100 | 4.3(-13) | 4.2(-13) | 4.9(-13) | 4.6(-13)                           | 4.4(-13) | 5.1(-13) | 4.9(-13)          |
| 1250 | 1.1(-12) | 1.0(-12) | 1.2(-12) | 1.1(-12)                           | 1.1(-12) | 1.2(-12) | 1.2(-12)          |
| 1500 | 3.4(-12) | 3.3(-12) | 3.6(-12) | 3.6(-12)                           | 3.6(-12) | 3.8(-12) | 3.8(-12)          |
| 1600 | 5.0(-12) | 4.9(-12) | 5.2(-12) | 5.3(-12)                           | 5.2(-12) | 5.5(-12) | 5.6(-12)          |
| 1700 | 7.0(-12) | 6.9(-12) | 7.2(-12) | 7.4(-12)                           | 7.3(-12) | 7.7(-12) | 8.0(-12)          |
| 1800 | 9.5(-12) | 9.3(-12) | 9.7(-12) | 1.0(-11)                           | 1.0(-11) | 1.1(-11) | 1.1(-11)          |
| 1900 | 1.3(-11) | 1.2(-11) | 1.3(-11) | 1.3(-11)                           | 1.3(-11) | 1.4(-11) | 1.5(-11)          |
| 1950 | 1.4(-11) | 1.4(-11) | 1.5(-11) | 1.5(-11)                           | 1.5(-11) | 1.6(-11) | 1.7(-11)          |
| 2000 | 1.6(-11) | 1.6(-11) | 1.6(-11) | 1.7(-11)                           | 1.7(-11) | 1.8(-11) | n.a.              |
| 2400 | 3.8(-11) | 3.7(-11) | 3.7(-11) | 4.1(-11)                           | 4.0(-11) | 4.1(-11) | n.a.              |

<sup>a</sup>the scaled frequencies are used in calculation of VaG, the calculation of vibrational partition functions, and the calculation of the effective mass for the small-curvature tunneling.

<sup>b</sup>from Ref. 8.

<sup>c</sup>n.a. denotes not available

Table 6-S. The specific reaction parameters (SRP) for MCOMP2, MC-QCISD, MCG3, and MCG2 in Tables 2-S to 5-S

|                       | $c_0$  | $c_1$  | $c_2$         | $c_3$         | $c_4$  | $c_5$  | $c_6$  | $c_7$  | Ref.              |
|-----------------------|--------|--------|---------------|---------------|--------|--------|--------|--------|-------------------|
| MCOMP2-SRP-15.1-3.3   | 0.9724 | 1.4775 | <b>0.7090</b> | <b>2.0067</b> |        |        |        |        | 22                |
| MC-QCISD-SRP-14.8-3.3 | 1.0038 | 1.3805 | <b>1.3508</b> | <b>1.0441</b> |        |        |        |        | p.w. <sup>a</sup> |
| MCG3-SRP-15.1-3.3     | 1.0054 | 0.9060 | <b>1.0907</b> | <b>1.2652</b> | 0.9272 | 0.4746 | 1.0165 | 1.5713 | p.w.              |

<sup>a</sup>denotes present work.



Table 6-S: contains the transition state geometries, vibrational frequencies for surfaces using methods presented in Table 2-S to Table 5-S.

Table 7-S: contains the vibrational frequencies for reactants and products on the surfaces using methods presented in Table 2-S to Table 5-S.

Table 8-S: gives the ZPE and barrier heights on the surfaces using methods presented in Table 2-S to Table 5-S.

Table 9-S: present multilevel coefficients for MCCM SRP presented in the supporting information.

Table 7-S. Rate constants ( $\text{cm}^3\text{molecule}^{-1}\text{s}^{-1}$ ) for MPW60 with all frequencies scaled by a factor of 0.96 and MPW60 with all principal force constants scaled by 0.92, both surfaces have a barrier height of 14.8 kcal/mol.

| T(K) | MPW60-FreqScaled-0.96 <sup>a</sup> |          |          | MPW60-FCScaled0.92 <sup>b</sup> |          |          | exp. <sup>c</sup> |
|------|------------------------------------|----------|----------|---------------------------------|----------|----------|-------------------|
|      | TST                                | CVT      | CVT/SCT  | TST                             | CVT      | CVT/SCT  |                   |
| 250  | 1.6(-22)                           | 1.2(-22) | 7.2(-21) | 1.6(-22)                        | 1.3(-22) | 7.6(-21) | n.a. <sup>d</sup> |
| 298  | 1.2(-20)                           | 9.7(-21) | 1.4(-19) | 1.3(-20)                        | 1.1(-20) | 1.5(-19) | n.a.              |
| 300  | 1.5(-20)                           | 1.1(-20) | 1.6(-19) | 1.5(-20)                        | 1.2(-20) | 1.7(-19) | n.a.              |
| 348  | 3.3(-19)                           | 2.7(-19) | 1.8(-18) | 3.3(-19)                        | 2.8(-19) | 1.8(-18) | 2.3(-18)          |
| 400  | 4.2(-18)                           | 3.6(-18) | 1.4(-17) | 4.2(-18)                        | 3.7(-18) | 1.4(-17) | 1.8(-17)          |
| 600  | 1.4(-15)                           | 1.3(-15) | 2.3(-15) | 1.4(-15)                        | 1.4(-15) | 2.4(-15) | 2.6(-15)          |
| 700  | 8.2(-15)                           | 7.7(-15) | 1.2(-14) | 8.1(-15)                        | 7.8(-15) | 1.2(-14) | 1.2(-14)          |
| 800  | 3.1(-14)                           | 3.0(-14) | 4.0(-14) | 3.1(-14)                        | 3.0(-14) | 4.1(-14) | 4.0(-14)          |
| 900  | 9.1(-14)                           | 8.7(-14) | 1.1(-13) | 9.0(-14)                        | 8.8(-14) | 1.1(-13) | 1.1(-13)          |
| 1000 | 2.2(-13)                           | 2.1(-13) | 2.5(-13) | 2.2(-13)                        | 2.1(-13) | 2.6(-13) | 2.4(-13)          |
| 1100 | 4.6(-13)                           | 4.4(-13) | 5.1(-13) | 4.5(-13)                        | 4.5(-13) | 5.2(-13) | 4.9(-13)          |
| 1250 | 1.1(-12)                           | 1.1(-12) | 1.2(-12) | 1.1(-12)                        | 1.1(-12) | 1.2(-12) | 1.2(-12)          |
| 1500 | 3.6(-12)                           | 3.6(-12) | 3.8(-12) | 3.6(-12)                        | 3.6(-12) | 3.8(-12) | 3.8(-12)          |
| 1600 | 5.3(-12)                           | 5.2(-12) | 5.5(-12) | 5.3(-12)                        | 5.2(-12) | 5.6(-12) | 5.6(-12)          |
| 1700 | 7.4(-12)                           | 7.3(-12) | 7.7(-12) | 7.4(-12)                        | 7.4(-12) | 7.7(-12) | 8.0(-12)          |
| 1800 | 1.0(-11)                           | 1.0(-11) | 1.1(-11) | 1.0(-11)                        | 1.0(-11) | 1.1(-11) | 1.1(-11)          |
| 1900 | 1.3(-11)                           | 1.3(-11) | 1.4(-11) | 1.3(-11)                        | 1.3(-11) | 1.4(-11) | 1.5(-11)          |
| 1950 | 1.5(-11)                           | 1.5(-11) | 1.6(-11) | 1.5(-11)                        | 1.5(-11) | 1.6(-11) | 1.7(-11)          |
| 2000 | 1.7(-11)                           | 1.7(-11) | 1.8(-11) | 1.7(-11)                        | 1.7(-11) | 1.8(-11) | n.a.              |
| 2400 | 4.1(-11)                           | 4.0(-11) | 4.1(-11) | 4.0(-11)                        | 4.0(-11) | 4.1(-11) | n.a.              |

<sup>a</sup>the scaled frequencies are used in calculation of  $V_a^G$ , the calculation of vibrational partition functions, and the calculation of the effective mass for the small-curvature tunneling.

<sup>b</sup>the principal force constants in redundant internal coordinates are scaled by 0.92

<sup>c</sup>from Ref. 8.

<sup>d</sup>n.a. denotes not available